PERGAMON

International Journal of Solids and Structures 38 (2001) 4235–4264

INTERNATIONAL JOURNAL OF SOLIDS and STRUCTURES

www.elsevier.com/locate/ijsolstr

Coupled effects of temperature gradient and oxidation on thermal stress in thermal barrier coating system

Y.C. Zhou [a,b,*], T. Hashida [a]

[a] *Fracture Research Institute, Tohoku University, 01 Aza-Aoba, Aramaki, Aobaku, Sendai 980-8579, Japan*

[b] *Institute of Fundamental Mechanics and Material Engineering, Xiangtan University, Xiangtan, Hunan 411105, People's Republic of China*

Received 28 December 1999; in revised form 26 July 2000

Abstract

The thermal stress fields in thermal barrier coating (TBC) system are studied in the present paper. The thermal stress fields are induced by the non-linear coupled effect of temperature gradient, oxidation, thermal fatigue, creep, morphology of TBC system as well as cooling rate. TBC system is assumed to be partially stabilized ZrO_2 by 8 wt.% Y_2O_3 (PSZ) or mullite over a NiCrAlY bond coat sprayed on nickel superalloy or steel substrate. The TBC system is a composite medium with four layers in cylindrical coordinate system. The temperature fields for the non-homogeneous problem with energy generation in medium are analytical solved by using Taylor transformation and Green's function approach. The analytical solutions for thermal stress fields in composite medium are obtained when eigenstrain rate is taken into consideration. The constitutive equations, such as the creep of ceramic coating (PSZ and mullite) and substrate (Ni-superalloy), plasticity of bond coat are given by a general formula. Thermal growth oxidation (TGO) and the temperature dependence of thermal–mechanical parameters are taken into consideration.

The calculated results of temperature fields and thermal stresses fields are given and the related results are discussed. TGO does not affect the temperature fields in PSZ coating systems. But it has influence on temperature fields in mullite coating systems. The residual stress with TGO considered is larger than that with TGO non-considered. It is very interesting to have the conclusion that TGO may make the residual tangent stress from tensile to compressive. The characterization of thermal stresses in PSZ coating system is very different from that in mullite coating system. It may be due to the difference of mechanical behavior such as creep, thermal mismatch as well as mechanical mismatch which is reflected by Dundurs' parameters $\overline{\alpha}$ and $\overline{\beta}$. The geometrical radius not only affects the quantum of thermal stress but also affects the characterization of thermal stress. The effect of cooling rate on residual stress is due to the high creep rate of ceramic coating operating at high temperature. The effect of cooling rate on residual stress is not large for system operating at relative low temperature.

Keywords: Thermal barrier coating; Thermal stress fields; Temperature gradient; Thermal growth oxidation

* Corresponding author. Fax: +81-22-217-4311.

E-mail address: zhou@rift.mech.tohoku.ac.jp (Y.C. Zhou).

0020-7683/01/$ - see front matter
PII: S0020-7683(00)00309-7

1. Introduction

There is a strong demand for mitigating the carbon dioxide emission, which is one of primary causes for global wasting effect. For fossil fuel fired power generation, the higher thermal efficiency is most effective for reducing carbon dioxide emission. Development of the advanced gas turbine will create the next generation electric power system (Amagasa et al., 1994; Yuri et al., 1997). The program included three developing parts: (1) high-performance and high-reliability turbine vanes and blades, (2) hot parts cooling technology, and (3) high temperature and low-NO_x combustor. The materials of high-performance and high-reliability include the high heat-resistance of new alloys and thermal barrier ceramic coating (TBC). The study of TBC is to develop a technology to protect alloy and make it to operate at 1500°C and to realize 50% of thermal efficiency. A TBC provides performance, efficiency, and durability benefits by reducing turbine cooling air requirements and lowering metal temperatures. Before TBC system is used, the following questions must be answered: How long does the TBC system service in the operational circumstance? Although there has been much research on the prediction of TBC service life, there is not any code or model that can clearly predict the service life of TBC system till now.

Previous research has demonstrated that there are some important effects on TBC operating life. The first is thermal fatigue (Takeuchi and Kokini, 1994; Kokini et al., 1996; Zhu and Miller, 1998, 1999; Jian et al., 1995). High temperature heating and low or fast cooling must induce thermal stress loading and unloading for many cycles. The second is thermal growth oxidation (TGO) between bond coat and thermal barrier ceramic coating (Cheng et al., 1998; Tolpygo et al., 1998; Ogawa et al., 1999; Tawancy et al., 1998; Gell et al., 1999). Generally, the composition of TGO is brittle ceramic, such as alumina (Al_2O_3). The cycles of high temperature loading and unloading not only make TGO to thicken but also make micro-voids and micro-cracks formation in TGO. On the other hand, the degradation of TGO may induce the spallation or delamination of thermal barrier ceramic coatings. The third is the surface roughness of bond coat (Cheng et al., 1998; Wang and Evans, 1999; He et al., 1998). The effect makes the formation of tensile stress at the peaks of interface undulation or compress stress at the valleys of interface undulation at cooling stage. The fourth is oxygen and sulfur penetration along grain boundaries (Bernstein and Allen, 1992). Their effect causes the thermal barrier ceramic coatings to thin and consequence the function of TBC is weakened.

There are many papers concerning the life prediction and failure mechanism of TBC system (Chaudhury et al., 1997; Rejda et al., 1997; Wesling et al., 1994; Cruse et al., 1988; Barlett and Maschio, 1995; Newaz et al., 1998; Wu et al., 1989, 1990; DeMasi-Marcin et al., 1990; Miller, 1989; Meier et al., 1992). As we know, the temperature gradient along TBC system thickness direction and TGO between bond coat and ceramic coating should have an important effect residual stress, thermal mechanical fatigue as well as creep of TBC system. Therefore, the service life of TBC system is governed by the non-linear coupled effect of temperature gradient, thermal growth oxidation, morphology of interface and the whole TBC system, thermal fatigue, creep as well as residual stress.

The purpose of the investigation is to study the thermal stress fields in TBC system. The thermal stress fields are induced by the non-linear coupled effect of temperature gradient, oxidation, thermal fatigue, creep, morphology of TBC system as well as cooling rate.

2. Theoretical model

For the study of failure mechanism of thermal barrier ceramic coating system operating at high temperature conditions, the physical map of temperature field and related thermal stress fields should be the first concerned problem. Generally, the problem should be three dimensional. For simplicity, two-dimensional problem is studied. Let us consider a cylindrical shell that comprises four layers as shown in Fig. 1. The innermost layer marked number 1 is substrate that is super-alloy. The outermost layer is thermal

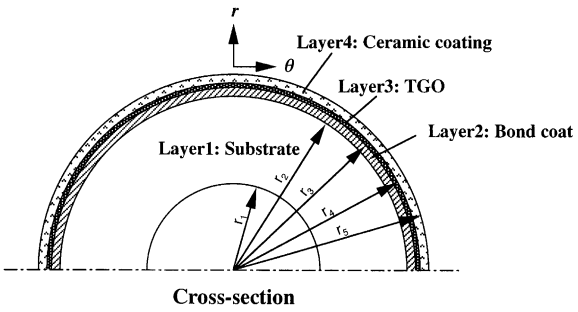

Fig. 1. Scheme of the theoretical model for thermal stress fields in TBC system.

barrier ceramic coating that is marked number 4. The second and third layers which are marked by numbers 2 and 3 are bond coat and thermal grown oxidation, respectively.

2.1. Temperature fields

2.1.1. Governing equations

In the determination of temperature fields, the following assumptions are given. (1) Energy is generated in layer i ($i = 1, 2, \ldots, M$) at a rate of $g_i(r, t)$ which may be induced by plastic work, where $M = 4$ for the interested problem as schemed in Fig. 1. (2) Thermal deformation is infinitesimal so that the temperature distribution can be solved based on initial configuration rather than on deformed ones. (3) Continuity of heat flux is across interface and contact conductance h_i at interfaces $r = r_i$ ($i = 1, 2, \ldots, M$) exists.

The governing equation for the transient temperature field $T_i(r, t)$ in layer i, $i = 1, 2, \ldots, M$ is

$$\rho_i c_{pi} \frac{\partial T_i}{\partial t} = \frac{1}{r} \frac{\partial}{\partial r} \left[r k_i(T_i) \frac{\partial T_i}{\partial r} \right] + g_i(r, t) \quad r_i < r < r_{i+1}, \quad i = 1, 2, \ldots, M \tag{1}$$

subject to the boundary conditions

$$\left[-k_1 \frac{\partial T_1}{\partial r} + h_1 T_1 \right] \Big|_{r=r_1} = h_1 f_1(t), \tag{2}$$

$$-k_i \frac{\partial T_i}{\partial r} \Big|_{r=r_{i+1}} = h_{i+1}(T_i - T_{i+1}) \Big|_{r=r_{i+1}}, \quad i = 1, 2, \ldots, M-1, \tag{3}$$

$$k_i \frac{\partial T_i}{\partial r} \Big|_{r=r_{i+1}} = k_{i+1} \frac{\partial T_{i+1}}{\partial r} \Big|_{r=r_{i+1}}, \quad i = 1, 2, \ldots, M-1, \tag{4}$$

$$\left[k_M \frac{\partial T_M}{\partial r} + h_{M+1} T_M \right] \Big|_{r=r_{M+1}} = h_{M+1} f_{M+1}(t), \tag{5}$$

and the initial conditions:

$$T_i(r, t)|_{t=0} = F_i(r), \quad r_i < r < r_{i+1}, \quad i = 1, 2, \ldots, M. \tag{6}$$

In the above equations, k, ρ, c_p are, respectively, thermal conductivity, mass density and specific heat, t is time. Boundary conditions (2) and (5) present heat supply or loss with convection from outer boundary surface $r = r_{M+1}$ in temperature $f_{M+1}(t)$ and inner boundary surface $r = r_1$ in temperature $f_1(t)$, with heat transfer coefficients h_{M+1} and h_1, respectively. First and second kind of boundary conditions will be

obtainable for outer or inner boundary surfaces by setting proper values for these coefficients. For example, for the first kind of boundary conditions $k_1 = 0$ and $f_1(t)$ is boundary temperature in Eq. (2).

2.1.2. Transformation of the equations

Generally, all thermal parameters, such as thermal conductivity, mass density and specific heat are temperature dependent. On the other hand, the thermal conductivity is more temperature-dependent than other thermal physical parameters. In order to consider the effect of temperature-dependent parameters on temperature fields, the following Taylor transformation is used,

$$\Theta_i(r,t) = \frac{1}{k_i(T_0)} \int_{T_0}^{T_i} k_i(\xi)\,\mathrm{d}\xi, \tag{7}$$

where T_0 is room temperature. Through Taylor transformation, the temperature fields governing Eqs. (1)–(6) are changed to the following equations with variable $\Theta_i(r,t)$:

$$\frac{\partial \Theta_i}{\partial t} = b_i(T_i)\frac{1}{r}\frac{\partial}{\partial r}\left(r\frac{\partial \Theta_i}{\partial r}\right) + \frac{b_i(T_i)}{k_i(T_i)}g_i(r,t), \quad r_i < r < r_{i+1} \;\; i = 1,2,\ldots,M \tag{8}$$

subject to the boundary conditions

$$\left[-k_1(T_0)\frac{\partial \Theta_1}{\partial r} + h_1(T_1)\Theta_1\right]\Big|_{r=r_1} = h_1(T_1)f_1(t), \tag{9}$$

$$-k_i(T_0)\frac{\partial \Theta_i}{\partial r}\Big|_{r=r_{i+1}} = h_{i+1}(\Theta_i - \Theta_{i+1})\Big|_{r=r_{i+1}}, \quad i = 1,2,\ldots,M-1, \tag{10}$$

$$k_i(T_0)\frac{\partial \Theta_i}{\partial r}\Big|_{r=r_{i+1}} = k_{i+1}(T_0)\frac{\partial \Theta_{i+1}}{\partial r}\Big|_{r=r_{i+1}}, \quad i = 1,2,\ldots,M-1, \tag{11}$$

$$\left[k_M(T_0)\frac{\partial \Theta_M}{\partial r} + h_{M+1}(T_M)\Theta_M\right]\Big|_{r=r_{M+1}} = h_{M+1}(T_M)f_{M+1}(t), \tag{12}$$

and the initial conditions:

$$\Theta_i(r,t)|_{t=0} = \frac{1}{k_i(T_0)}\int_{T_0}^{F_i(r)} k_i(\xi)\,\mathrm{d}\xi = \gamma_i(r), \quad r_i < r < r_{i+1} \;\; i = 1,2,\ldots,M. \tag{13}$$

In the above equations, such as Eqs. (9)–(11), zero-order approximation is used for T_i replaced by Θ_i. In Eq. (8), $b_i(T_i) = (k_i(T_i))/(\rho_i(T_i)c_{pi}(T_i))$ is thermal diffusivity.

2.1.3. Solution of temperature fields

The above equations about temperature field are a problem with non-homogeneous boundary conditions. The problem should be transformed into the one with homogeneous boundary conditions (Özisik, 1993). Generally, the orthogonal expansion technique is used to solve the homogeneous problem of composite medium of finite thickness, while the Laplace transformation is used to solve the homogeneous problem of composite medium of infinite and semi-infinite thickness. The Green's function approach is used for solving the non-homogeneous problem with energy generation in medium.

In order to transform the time-dependent problem into a one with homogeneous boundary conditions, we consider $\Theta_i(r,t)$ constructed by the superposition of three simple problems in the form:

$$\Theta_i(r,t) = \vartheta_i(r,t) + \phi_i(r)f_1(t) + \psi_i(r)f_{M+1}(t), \tag{14}$$

where the functions $\phi_i(r)$, $\psi_i(r)$ and $\vartheta_i(r)$ are given in Appendix A.

2.2. Thermal stress fields

2.2.1. Governing equations

Thermal stresses are considered to be two-dimensional problem for thermal barrier ceramic coating system. The general Hook's constitutive relation in two-dimensional state can be written in rate form as

$$\dot{\varepsilon}_{rr} = \frac{1}{2\mu}\left[\dot{\sigma}_{rr} - \frac{1}{4}(3-\kappa)(\dot{\sigma}_{rr} + \dot{\sigma}_{\vartheta\vartheta})\right] + \dot{E}_{rr} + \eta\dot{E}_{zz}, \tag{15}$$

$$\dot{\varepsilon}_{r\vartheta} = \frac{1}{2\mu}\dot{\sigma}_{r\vartheta} + \dot{E}_{r\vartheta}, \tag{16}$$

$$\dot{\varepsilon}_{\vartheta\vartheta} = \frac{1}{2\mu}\left[\dot{\sigma}_{\vartheta\vartheta} - \frac{1}{4}(3-\kappa)(\dot{\sigma}_{rr} + \dot{\sigma}_{\vartheta\vartheta})\right] + \dot{E}_{\vartheta\vartheta} + \eta\dot{E}_{zz}. \tag{17}$$

In the above equations, $\dot{E}$ is used to denote the eigenstrain rate which maybe plastic strain rate, thermal expansion strain rate, etc., as defined by Mura (1982). The eigenstrain rate $\dot{E}_{zz}$ is the normal strain rate perpendicular to the plane that is interested. Moreover, v denotes Poisson's ratio $\kappa = 3 - 4v$, $\eta = v$ for plane strain, and $\kappa = (3-v)/(1+v)$, $\eta = 0$ for plane stress.

2.2.2. The general solution for the displacement rate field

Due to axisymmetry, the displacement rate in r, ϑ directions can be expressed as $\dot{u}_r = \dot{u}(r,t)$, $\dot{u}_\vartheta = 0$. In this case, by using the well-known equations of equilibrium equations and strain rate-displacement relations, the governing equations are readily obtained in terms of displacement rate $\dot{u}$:

$$\frac{\partial}{\partial r}\left[\frac{1}{r}\frac{\partial}{\partial r}(r\dot{u})\right] = \mathrm{X}(r,t), \tag{18}$$

where

$$\begin{aligned}\mathrm{X}(r,t) = {} & \frac{1}{\kappa+1}\left\{\left[(\kappa+1)\frac{\partial}{\partial r} + 2(\kappa-1)\frac{1}{r}\right](\dot{E}_{rr} + \eta\dot{E}_{zz}) + \left[(3-\kappa)\frac{\partial}{\partial r} - 2(\kappa-1)\frac{1}{r}\right](\dot{E}_{\vartheta\vartheta} + \eta\dot{E}_{zz})\right\} \\ & - \frac{\kappa-1}{(\kappa+1)\mu}\left\{\left[\frac{\partial\dot{u}}{\partial r} - (\dot{E}_{rr} + \eta\dot{E}_{zz})\right]\frac{\partial}{\partial r}\left(\frac{\kappa+1}{\kappa-1}\mu\right) + \left[\frac{\dot{u}}{r} - (\dot{E}_{\vartheta\vartheta} + \eta\dot{E}_{zz})\right]\frac{\partial}{\partial r}\left(\frac{3-\kappa}{\kappa-1}\mu\right)\right\}.\end{aligned} \tag{19}$$

The general solution to the above equation is given by

$$\dot{u}(r,t) = Ar + \frac{B}{r} + \frac{r}{2}\int \mathrm{X}(r,t)\,\mathrm{d}r - \frac{1}{2r}\int r^2\mathrm{X}(r,t)\,\mathrm{d}r, \tag{20}$$

where A and B are integral constants which are determined by boundary conditions for the composite medium of finite thickness. The expression of displacement rate $\dot{u}$ for layer i can be written as

$$\dot{u}_i(r,t) = A_i r + \frac{B_i}{r} + rC_i(r,t) + \frac{D_i(r,t)}{r}, \tag{21}$$

where

$$C_i(r,t) = \frac{1}{2}\int_{r_i}^{r}\mathrm{X}_i(\zeta,t)\,\mathrm{d}\zeta, \quad D_i(r,t) = -\frac{1}{2}\int_{r_i}^{r}\zeta^2\mathrm{X}_i(\zeta,t)\,\mathrm{d}\zeta, \qquad r \in [r_i, r_{i+1}]. \tag{22}$$

From the above equations,

$$\dot{\sigma}_{rri} = \frac{4\mu_i}{\kappa_i - 1}\left[A_i + \frac{1}{2}(1-\kappa_i)\frac{B_i}{r^2} + C_i(r,t) + \frac{1}{2}(1-\kappa_i)\frac{D_i(r,t)}{r^2} - E_i(r,t)\right], \tag{23}$$

where

$$E(r,t) = \frac{\kappa+1}{4}(\dot{E}_{rr} + \eta\dot{E}_{zz}) + \frac{3-\kappa}{4}(\dot{E}_{\vartheta\vartheta} + \eta\dot{E}_{zz}). \tag{24}$$

2.2.3. Boundary conditions at interfaces and on the outer surface

Generally, the boundary condition at a bonded interface between two phases is that traction and displacements are to be continuous. Continuity of traction is nothing else but Newton's third law and should not be touched. Continuity of displacements is another matter. For example, the interface may slip or no frictionless slip for the interface that is not bonded enough. In this case, the displacement may not be continuous. Dundurs (1990) gave the boundary conditions at interfaces by thinking in terms of stretch strains and curvature changes. The traction and displacement are continuous at interfaces for the bonded interface condition. The boundary conditions at a geometrically smooth interface between two bonded phases are written as

$$\dot{\sigma}_{rri}(r_{i+1},t) = \dot{\sigma}_{rri+1}(r_{i+1},t), \quad i = 1,2,\ldots,M-1, \tag{25}$$

$$\dot{\sigma}_{r\vartheta i}(r_{i+1},t) = \dot{\sigma}_{r\vartheta i+1}(r_{i+1},t), \quad i = 1,2,\ldots,M-1, \tag{26}$$

$$\dot{\varepsilon}_{\vartheta\vartheta i}(r_{i+1},t) = \dot{\varepsilon}_{\vartheta\vartheta i+1}(r_{i+1},t), \quad i = 1,2,\ldots,M-1, \tag{27}$$

$$\Delta\dot{K}_i(r_{i+1},t) = \Delta\dot{K}_{i+1}(r_{i+1},t), \quad i = 1,2,\ldots,M-1. \tag{28}$$

In the above equations, K is the curvature. Therefore, Eq. (28) means the continuity of curvature change at the interface. However, for a frictionless slipping interface, Eq. (27) does not exist and the shear stress $\sigma_{r\vartheta}$ should vanish.

For the present axisymmetrical problem, the shear stresses $\sigma_{r\vartheta}$ vanish. The Eqs. (27) and (28) become to be identical, that is the continuity of displacements at the interface. Therefore, the boundary conditions at a geometrically smooth interface between two phases are finally written as

$$\begin{aligned} \dot{\sigma}_{rri}(r_{i+1},t) &= \dot{\sigma}_{rri+1}(r_{i+1},t), \quad i = 1,2,\ldots,M-1, \\ \dot{u}_i(r_{i+1},t) &= \dot{u}_{i+1}(r_{i+1},t), \quad i = 1,2,\ldots,M-1. \end{aligned} \tag{29}$$

For both of the bonded interface and frictionless slipping interface boundary conditions, outer surface and inner surface are stress free:

$$\dot{\sigma}_{rr1}(r_1,t) = 0, \qquad \dot{\sigma}_{rrM}(r_{M+1},t) = 0. \tag{30}$$

The related $2M$ constants A_i and B_i for $i = 1,2,\ldots,M$ in Eqs. (21) and (23) can be determined by the $2M$ linear equations which are $2(M-1)$ boundary conditions at interface described by Eqs. (25) and (29) and two boundary conditions described by Eq. (30). The $2M$ constants A_i and B_i for $i = 1,2,\ldots,M$ are given in Appendix B.

3. Constitutive equations and thermal growth oxidation

3.1. Constitutive equations

The constitutive equation is a basic physical equation and it is essential for studying thermal stresses in TBC system. The rate of deformation tensor $\mathbf{D}$ defined as the symmetric part of $\dot{\mathbf{F}}\cdot\dot{\mathbf{F}}^{-1}$, where $\mathbf{F}$ is deformation gradient, can be decomposed into an elastic part $\mathbf{D}^{\mathrm{e}}$ and an eigen part $\mathbf{D}^{\mathrm{eig}}$,

$$\mathbf{D}=\mathbf{D}^{\mathrm{e}}+\mathbf{D}^{\mathrm{eig}}. \tag{31}$$

The rate of elastic deformation is given by

$$\mathbf{D}^{\mathrm{e}}=\frac{1}{2\mu}\left[\hat{\boldsymbol{\sigma}}-\frac{v}{1+v}(\hat{\boldsymbol{\sigma}}:\mathbf{I})\mathbf{I}\right], \tag{32}$$

where $\mathbf{I}$ is second-order identity tensor and the notation $\mathbf{A}$:$\mathbf{B}$ denotes dyadic product between tensor $\mathbf{A}$ and $\mathbf{B}$. In Eq. (31), $\mathbf{D}^{\mathrm{e}}$ is a linear function of the objective stress rate of Cauchy tensor $\hat{\boldsymbol{\sigma}}$, which is expressed by

$$\hat{\boldsymbol{\sigma}}=\dot{\boldsymbol{\sigma}}+\boldsymbol{\sigma}\cdot\mathbf{W}-\mathbf{W}\cdot\boldsymbol{\sigma}, \tag{33}$$

where the dot over a character signifies the material time derivative:

$$\dot{\boldsymbol{\sigma}}=\frac{\partial\boldsymbol{\sigma}}{\partial t}+\mathbf{v}\cdot(\operatorname{grad}\boldsymbol{\sigma}), \tag{34}$$

and $\mathbf{W}$ is consider as a generalized spin tensor and $\mathbf{v}$ the particle velocity.

The rate of deformation tensor for eigen part $\mathbf{D}^{\mathrm{eig}}$ is decomposed into creep strain rate tensor $\mathbf{D}^{\mathrm{creep}}$, plastic strain rate tensor $\mathbf{D}^{\mathrm{p}}$ and temperature rise rate tensor $\mathbf{D}^{\mathrm{temp}}$. It is assumed that the material is isotropy, therefore, the temperature rise rate tensor is written as

$$\mathbf{D}^{\mathrm{temp}}=\alpha\dot{T}\mathbf{I}, \tag{35}$$

where α is thermal expansion coefficient. The partial differentials of creep potential function f or plastic potential f in stress space give the creep rate tensor $\mathbf{D}^{\mathrm{creep}}$ or plastic strain rate tensor $\mathbf{D}^{\mathrm{p}}$ which is designated by $\mathbf{D}^{\mathrm{in}}$ as

$$\mathbf{D}^{\mathrm{in}}=\Lambda\frac{\partial f}{\partial\boldsymbol{\sigma}}, \tag{36}$$

where Λ is a proportionality factor. Squaring the above equation leads to

$$D_2^{\mathrm{in}}=\frac{1}{2}\Lambda^2\frac{\partial f}{\partial\boldsymbol{\sigma}}:\frac{\partial f}{\partial\boldsymbol{\sigma}}=\frac{1}{2}\Lambda^2 J_2, \tag{37}$$

where D_2^{in} and J_2 are, respectively, the creep strain rate invariant (or plastic strain rate invariant) and deviator stress tensor $\mathbf{S}$ invariant. They are given by

$$D_2^{\mathrm{in}}=\tfrac{1}{2}\mathbf{D}^{\mathrm{in}}:\mathbf{D}^{\mathrm{in}},\qquad J_2=\tfrac{1}{2}\mathbf{S}:\mathbf{S}. \tag{38}$$

Generally, the relation governing creep strain rate or plastic strain rate is obtained by experiment test for one-dimensional shape sample. In order to obtain the relation of D_2^{in} with J_2 by one-dimensional tensile or compressive experiment $\sqrt{D_2^{\mathrm{in}}}$ is thought to be equivalent creep strain rate or plastic strain rate and $\sqrt{J_2}$ is thought to be equivalent stress (Zhou et al., 1997). By comparing Eq. (37) with one-dimensional tensile or compressive experiment, the proportionality factor Λ in Eq. (37) can be obtained. Once the proportionality factor Λ is known, the creep or plastic strain rate tensor $\mathbf{D}^{\mathrm{in}}$ for Eq. (36) can be obtained. Finally, the eigenstrain rate tensor $\mathbf{D}^{\mathrm{eig}}$ in Eqs. (15)–(17) can be obtained.

3.2. Creep constitutive equations

As discussed above, when one-dimensional relation of creep rate with stress is tested, three-dimensional creep constitutive equation can be derived. In the present study, the creep strain rates for ceramic coating and substrate superalloy are given based on the ideas. Generally the constitutive relation for ceramic coating and substrate superalloy can be unifiedly written as

$$D_2^{\text{creep}} = \Pi \exp\left(-\frac{Q}{RT}\right)\left(\frac{\sqrt{3J_2}}{\sigma_0}\right)^n\left(\frac{t}{t_0}\right)^{-s}, \tag{39}$$

where Π, Q, n and s are, respectively, material constant, activation energy, stress exponent and time exponent. R is gas constant. T and t are, temperature and time, respectively. σ_0 and t_0 are, reference stress and reference time, respectively.

3.3. Plastic constitutive equations

It is assumed that one-dimensional stress–strain relation for loading state is expressed by

$$\bar{\varepsilon} = f_0(\bar{\sigma}), \tag{40}$$

where $\bar{\varepsilon}$ and $\bar{\sigma}$ are, respectively, equivalent effective strain and stress. Therefore, Eq. (37) can be written as

$$D_2^{\text{p}} = \left(\frac{\partial f_0}{\partial \bar{\sigma}} - \frac{1}{E}\right)\frac{\mathrm{d}\bar{\sigma}}{\mathrm{d}t} \quad \text{for loading state,} \tag{41}$$

$$D_2^{\text{p}} = 0 \quad \text{for unloading state.} \tag{42}$$

In the above equations, the criterion of loading or unloading is expressed as $F \geqslant 0$ for loading and $F < 0$ for unloading, where

$$F = \frac{3}{2\bar{\sigma}}\left[1 - \frac{1}{E}\frac{1}{\mathrm{d}f_0(\bar{\sigma})/\mathrm{d}\bar{\sigma}}\right]\left[(\sigma_{rr} - \sigma_m)\dot{\sigma}_{rr} + (\sigma_{\vartheta\vartheta} - \sigma_m)\dot{\sigma}_{\vartheta\vartheta} + \sigma_{r\vartheta}\dot{\sigma}_{r\vartheta}\right]. \tag{43}$$

3.4. Unified eigenstrain rate

Combing the above sections, the unified eigenstrain rate in Eqs. (15)–(17) can be written in the following form:

$$\dot{E}_{rr} = \frac{3(\sigma_{rr} - \sigma_m)}{2\bar{\sigma}}\Pi \exp\left(-\frac{Q}{RT}\right)\left(\frac{\bar{\sigma}}{\sigma_0}\right)^n\left(\frac{t}{t_0}\right)^{-s} + \frac{3(\sigma_{rr} - \sigma_m)}{2\bar{\sigma}}D_2^{\text{p}} + \alpha\dot{T}, \tag{44}$$

$$\dot{E}_{r\vartheta} = \frac{3\sigma_{r\vartheta}}{2\bar{\sigma}}\Pi \exp\left(-\frac{Q}{RT}\right)\left(\frac{\bar{\sigma}}{\sigma_0}\right)^n\left(\frac{t}{t_0}\right)^{-s} + \frac{3\sigma_{r\vartheta}}{2\bar{\sigma}}D_2^{\text{p}}, \tag{45}$$

$$\dot{E}_{\vartheta\vartheta} = \frac{3(\sigma_{\vartheta\vartheta} - \sigma_m)}{2\bar{\sigma}}\Pi \exp\left(-\frac{Q}{RT}\right)\left(\frac{\bar{\sigma}}{\sigma_0}\right)^n\left(\frac{t}{t_0}\right)^{-s} + \frac{3(\sigma_{\vartheta\vartheta} - \sigma_m)}{2\bar{\sigma}}D_2^{\text{p}} + \alpha\dot{T}, \tag{46}$$

where σ_m is average stress. In the above expressions, the first term, second term and third term on the left side are, respectively, the contribution of creep strain rate, plastic strain rate and temperature rise rate to eigenstrain rate.

3.5. Thermal growth oxidation

As we know, for TBC system operating at high temperature with long time the localized oxidation between ceramic top coat/metallic (NiCrAlY) bond coat interface will take place. Oxidation of bond coat has been repeatedly identified as one of the important factors affecting the ceramic top coating durability during services. Some researchers have investigated the oxidation generation processing, oxidation thickness as well as the life prediction of TBC system based on thermally grown oxidation. However, the mechanisms by which oxidation facilitate TBC failure are poorly understood and require further characterization. In the present investigation, it is assumed that the mixed layer exist between the bond coat and top ceramic coating before the oxidation layer completely formation based on the experimental observation (Ogawa et al., 1999). The mixed layer is the composites of Al_2O_3 and bond coat and the chemical compositions in the mixed layer are change as time progress. The thickness of thermally grown oxidation is obtained by fitting the experimental data (Itoh et al., 1998) as

$$\omega = \lambda_0 t^{\lambda_1}, \tag{47}$$

where ω is TGO thickness with unit of μm and t is time with unit of s. λ_0 and λ_1 are parameters,

$$\lambda_0 = 10^{((a_0/T)+b_0)}\mu\mathrm{m/s}^{-0.45}, \tag{48}$$

where $a_0 = -4150$, $b_0 = 1.154$ and T is temperature with unit of K. The parameter of λ_1 is 0.45. Therefore, the thermally grown oxidation rate is written as

$$\frac{\mathrm{d}\omega}{\mathrm{d}t} = \lambda_0\lambda_1\left(\frac{\omega}{\lambda_0}\right)^{1-(1/\lambda_1)}. \tag{49}$$

4. Calculated results and discussion

In this section, the results concerning thermal stress fields for TBC system operating at high temperature conditions are given as detailed as possible. The TBC system is schemed in Fig. 1. The ceramic coating system is assumed to be partially stabilized ZrO_2 by 8 wt.% Y_2O_3 or mullite over a NiCrAlY bond coat sprayed on nickel superalloy or steel substrate. In order to investigate the effect of different materials combinations on the failure mechanism of TBC system, the following four different combinations are studied: PSZ/Ni-alloy system, PSZ coating over a NiCrAlY bond coat on Ni-superalloy substrate; Mullite/Ni-alloy system, mullite coating over a NiCrAlY bond coat on Ni-superalloy substrate; PSZ/Steel system, PSZ coating over a NiCrAlY bond coat on steel substrate; Mullite/Steel system, mullite coating over a NiCrAlY bond coat on steel substrate. In the following discussion, interface 1, 2 and 3 are defined as the interfaces of substrate/bond-coat, bond-coat/TGO and TGO/TBC, respectively.

The thickness of substrate, bond coat and ceramic coating is, respectively, 0.20, 0.01 and 0.035 cm. The inner radius of the cylindrical shell is 0.2 cm. In order to investigate the effect of TGO on the failure mechanism of TBC system, the initial thickness of TGO is assumed to be 45 μm and the evolution of TGO thickness is given in Eq. (49). The system is thought to be a problem of plan strain.

4.1. Thermal physical parameters

Generally, thermal–physical parameters are all temperature dependent. Due to the transformation of expression (7), only two temperature-dependent parameters determine the temperature fields for TBC system. The two parameters are thermal diffusivity $b_i(T_i)$ in heat conduction equation (8) and thermal

Table 1
Thermal conductivity k ($W\,cm^{-1}\,K$)

Temperature (°C)	Substrate		Bond coat	TGO	TBC	
	Ni-alloy	Steel			PSZ	Mullite
20	0.880	0.1647	0.058	0.1000	1.956×10^{-2}	5.160×10^{-2}
200	0.733	0.1647	0.075	7.794×10^{-2}	1.834×10^{-2}	4.915×10^{-2}
400	0.595	0.1647	0.095	6.029×10^{-2}	1.736×10^{-2}	4.627×10^{-2}
600	0.620	0.1647	0.120	5.074×10^{-2}	1.627×10^{-2}	4.254×10^{-2}
800	0.650	0.1647	0.145	4.412×10^{-2}	1.634×10^{-2}	3.729×10^{-2}
1000	0.681	0.1647	0.162	4.412×10^{-2}	1.681×10^{-2}	1.186×10^{-2}
1100	0.690	0.1647	0.170	4.000×10^{-2}	1.700×10^{-2}	3.600×10^{-3}

Table 2
Thermal diffusivity ($cm^2\,s^{-1}$)

Temperature (°C)	Substrate		Bond coat	TGO	TBC	
	Ni-alloy	Steel			PSZ	Mullite
20	0.216	0.041	20.2	3.017×10^{-2}	7.500×10^{-3}	3.81×10^{-3}
200	0.160	0.041	23.0	2.351×10^{-2}	5.882×10^{-3}	3.07×10^{-3}
400	0.099	0.041	26.0	1.819×10^{-2}	5.147×10^{-3}	2.61×10^{-3}
600	0.131	0.041	28.5	1.531×10^{-2}	4.706×10^{-3}	2.30×10^{-3}
800	0.130	0.041	30.7	1.331×10^{-2}	4.647×10^{-3}	1.93×10^{-3}
1000	0.127	0.041	32.5	1.242×10^{-2}	4.706×10^{-3}	6.00×10^{-4}
1100	0.125	0.041	33.5	1.207×10^{-2}	4.706×10^{-3}	1.80×10^{-4}

conductivity $k_i(T_i)$ in transformation (7). The thermal conductivity and diffusivity for TBC system are listed in Tables 1 and 2, respectively. The thermal physical parameters for PSZ are obtained by analyzing the experimental results of Hasselman et al. (1987), An et al. (1985) and Chung et al. (1985). The thermal physical parameters for bond coat, i.e., NiCrAlY, are obtained by analyzing the experimental results of Chung et al. (1985). Generally, thermally grown oxidation is so thin that the size effect is very important. The thermal conductivity for thin TGO appears to have significantly lower thermal conductivity levels compared to bulk materials at room temperature. For instance, electron-beam-evaporated Al_2O_3 films a few micrometers thick and anodized Al_2O_3 coatings $\leqslant 100$ μm thick had thermal conductivity values almost an order of magnitude lower than the bulk materials (An et al., 1999). Considering the size effect reported in An et al. (1999) and Rohde (1997), the parameters of thermal conductivity for TGO are obtained from the results of Taylor (1998). The parameters of mass density and specific heat for TGO are obtained from the results of Glandus and Tranchand (1993). The thermal physical parameters for mullite and nickel superalloy substrate are taken from Schneider et al. (1994) and Betteridge (1984), respectively. Therefore, the thermal diffusivity can be calculated and the results are listed in Tables 1 and 2.

4.2. Mechanical physical parameters

Young's modulus, Poisson's ratio and thermal expansion coefficient for substrate such as Ni-superalloy and steel, bond coat NiCrAlY, TGO Al_2O_3 and ceramic coating, such as PSZ and mullite are listed in Tables 3–5, respectively. The mechanical parameters for substrate, bond coat, TGO and PSZ were taken from Cheng et al., (1998) and the parameters for mullite were taken from Kokini et al. (1996).

In the calculation, the ceramic coating, such as PSZ and mullite, is considered to be elastic and creep. The constants of creep for PSZ and mullite are taken from Thurn et al. (1997) and Kokini and Takeuchi

Table 3
Young's modulus (GPa)

Temperature (°C)	Substrate		Bond coat	TGO	TBC	
	Ni-alloy	Steel			PSZ	Mullite
20	220	207	200	400	48	30
200	210	207	190	390	47	30
400	190	207	175	380	44	30
600	170	207	160	370	40	30
800	155	207	145	355	34	30
1000	130	207	120	325	26	30
1100	120	207	110	320	22	30

Table 4
Poisson's ratio

Temperature (°C)	Substrate		Bond coat	TGO	TBC	
	Ni-alloy	Steel			PSZ	Mullite
20	0.31	0.33	0.30	0.23	0.10	0.20
200	0.32	0.33	0.30	0.23	0.10	0.20
400	0.33	0.33	0.31	0.24	0.10	0.20
600	0.33	0.33	0.31	0.24	0.11	0.20
800	0.34	0.33	0.32	0.25	0.11	0.20
1000	0.35	0.33	0.33	0.25	0.12	0.20
1100	0.35	0.33	0.33	0.25	0.12	0.20

Table 5
Thermal expansion coefficient ($\times 10^{-6}$/°C)

Temperature (°C)	Substrate		Bond coat	TGO	TBC	
	Ni-alloy	Steel			PSZ	Mullite
20	14.8	15.0	13.6	8.0	9.0	4.5
200	15.2	15.0	14.2	8.2	9.2	4.5
400	15.6	15.0	14.6	8.4	9.6	4.5
600	16.2	15.0	15.2	8.7	10.1	4.5
800	16.9	15.0	16.1	9.0	10.8	4.5
1000	17.5	15.0	17.2	9.3	11.7	4.5
1100	18.0	15.0	17.6	9.6	12.2	4.5

Table 6
The parameters of creep

Constants	Π (s^{-1})	Q (kJ mol^{-1})	n	σ_0 (MPa)	S	t_0 (s)
PSZ	0.405	114	0.48	1.0	0.82	1.0
Mullite	3.42×10^{-2}	748	1.0	1.0	0.0	1.0
Ni-alloy	3.72×10^{-49}	0.0	14.4	1.0	0.0	1.0

(1996), respectively. The related constants are listed in Table 6. TGO is considered to be elastic. The bond coat is considered to be elastic–perfectly plastic or linear hardening. The parameters of temperature-dependent yield for bond coat were taken from Cheng et al. (1998) and the parameters are listed in Table 7. The linear hardening modulus for bond coat is taken as 10.0 GPA. The substrate of Ni-superalloy is considered to be plastic and creep. The one-dimensional stress–strain relation in Eq. (42) for substrate

Table 7
Bond coat non-linear behavior

Temperature (°C)	Yield strength (Mpa)
20	426
200	412
400	396
600	362
800	284
1000	202
1100	114

nickel base superalloy is obtained from the test results of Hyde et al. (1997). The constants of creep for substrate Ni-superalloy are taken from Tabuchi et al. (1999). But the substrate of steel is considered to be elastic and the parameters are taken from Nusier and Newaz (1998).

4.3. Temperature fields without thermal grown oxidation

In the present investigation, only first or second kind of boundary conditions is considered. The outer surface is at the state of heating, high temperature hold and low or fast cooling. The inner surface is at the state of heat insulation for time early 1200 s and after that time the surface is on the state of first kind of condition. The temperature histories on outer and inner surfaces are shown in Fig. 2, where only first cycle temperature histories are shown. The highest temperature for coating surface is 1000°C and the lowest temperature for substrate surface is 700°C. The temperature histories for the boundary conditions are a typical operating state for TBC system (Jian, 1996). Besides the continuity of heat flux across the interface described by Eq. (3), the temperature was assumed to be continuous across the interface, i.e., perfect thermal contact between two layers at interface. This means that the coefficient h_{i+1} in Eq. (3) is infinite. On the other hand, the heat source is not considered.

Besides the histories of temperature on inner and outer surface, the temperature histories on interfaces for different combinations of TBC system are also shown in Fig. 2. The spatial distributions of temperature are shown in Fig. 3 at different time for different combinations of TBC. We can obtain the following results by observing Figs. 2 and 3. First, although the inner surface is heat insulated, the temperature difference between outer surface and inner surface is very little for time early 1200 s as shown in Fig. 3(a). The maximum temperature difference exists in system 3, i.e., PSZ/Ni-superalloy, which is 2.22°C is shown in

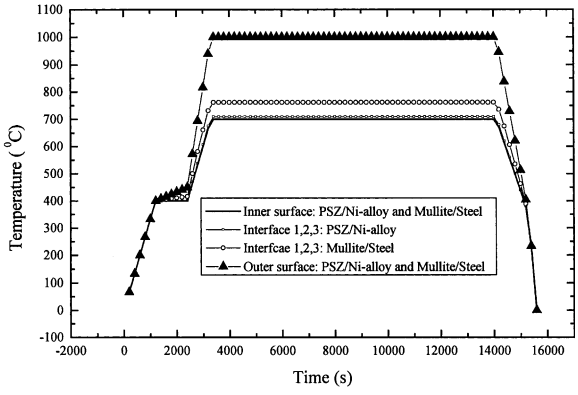

Fig. 2. Boundary conditions of temperature and histories of temperature at interfaces, where TGO is not considered.

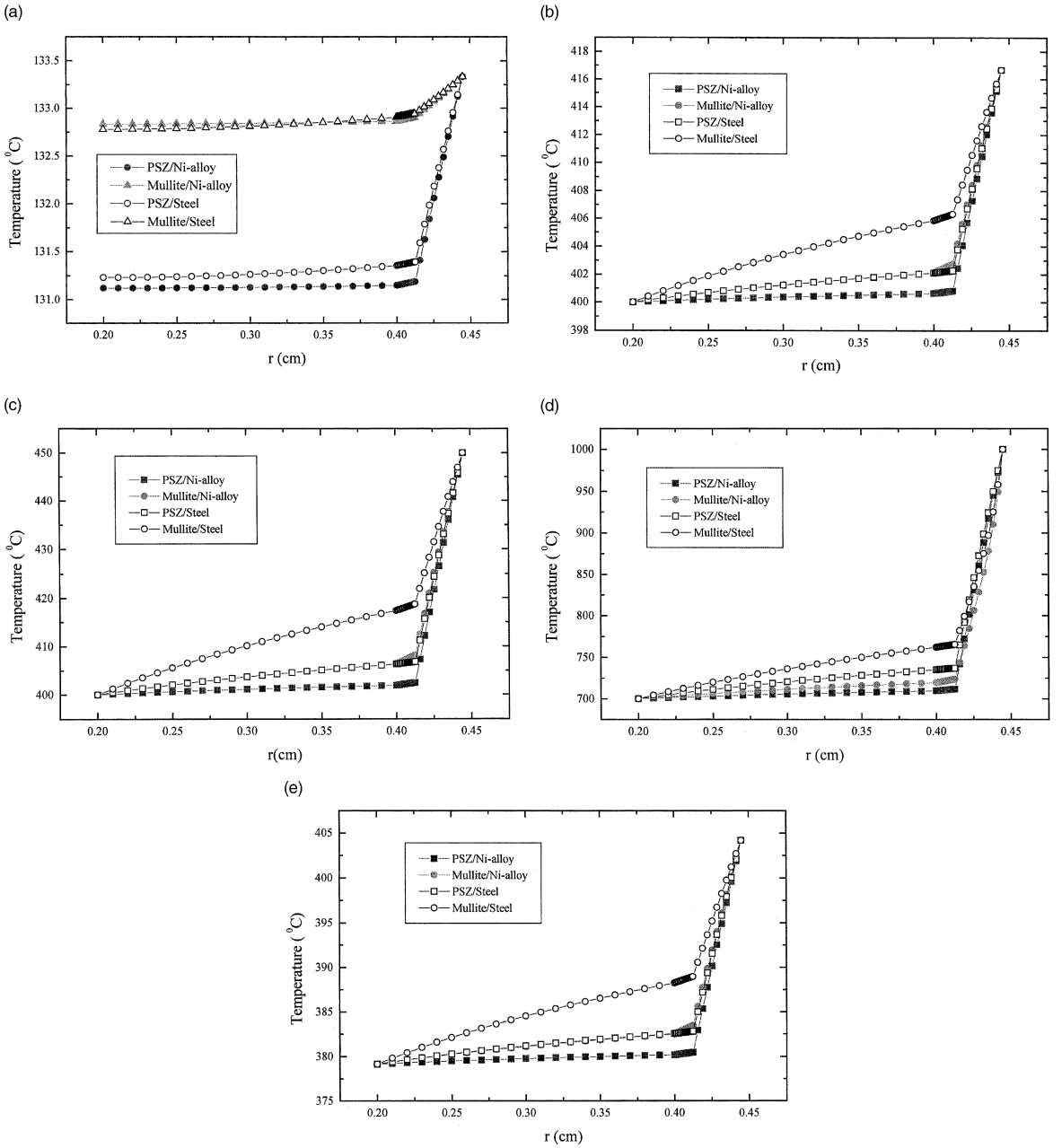

Fig. 3. Spatial distributions of temperature at different times: (a) 400, (b) 1600, (c) 2400, (d) 14 000, and (e) 15 200 s, where TGO is not considered.

Figs. 2 and 3(a). Second, the temperature spatial distributions are very different for different combinations of TBCs system. This is due to the difference of thermal physical parameters for different combinations of TBCs system. The largest temperature difference for ceramic coating exists in PSZ/Ni-alloy system and that is 288.31°C shown in Fig. 3(d) in the period of heat hold. The least temperature difference for ceramic

coating exists in mullite/steel system, and that is 234.79°C. The highest temperature difference for substrate exists in Mullite/Steel system, and that is 61.96°C in the period of heat hold. The least temperature difference exists in PSZ/Ni-alloy system, and that is 9.57°C. The highest temperature encountered to substrate is 709.57°C for PSZ/Ni-alloy system, however, it is 761.97°C for Mullite/Steel system. Therefore, PSZ/Ni-alloy system is optimum combination only if temperature field is considered for TBCs system operating at above typical condition.

4.4. Temperature fields with thermal growth oxidation

The spatial distributions of temperature at a typical time in heat hold period, i.e., at 14 000 s are shown in Fig. 4. The difference of temperature spatial distribution cannot be seen for PSZ/Ni-alloy system with and without considering TGO. The difference of temperature spatial distribution is little for PSZ/Steel system with and without considering TGO. However, the difference of temperature spatial distribution can be visualized in Fig. 4 for Mullite/Ni-alloy and Mullite/Steel systems with and without considering TGO. The temperature difference in substrate for Mullite/Steel system without considering TGO is 61.96°C and 91.53°C with considering TGO.

4.5. Thermal stress for TBCs system at elastic state

Let us study the radial or tangent stress histories and spatial distribution for a typical TBC system, i.e., PSZ/Ni-alloy system at elastic state. First, the radial stresses are discussed. The histories of radial stress at interfaces 1, 2 and 3 are shown in Fig. 5. At very early stage of heating, the radial stresses in interface are both tensile without and with considering TGO. But the state of tensile radial stress maintains less than 8 s. After that time, the stresses are compressive in interfaces in the period of heating and heat hold. However, the radial stresses become tensile on the end of cooling for every cycle of heating/cooling. The tensile stresses are due to the mismatch of thermal expansion and are called residual stresses. The residual elastic tensile stress is very little for TGO non-considered. The residual tensile stresses for TGO considered are larger than that for TGO non-considered as shown in Fig. 6. It is also seen that the residual stresses for TGO effect at interface 1 are much larger than that at interface 3. Fig. 7(a) and (b) show the spatial distribution of radial stress for TGO non-considered and TGO considered at different time. It is seen that the maximum compressive or tensile stresses do exist at interfaces.

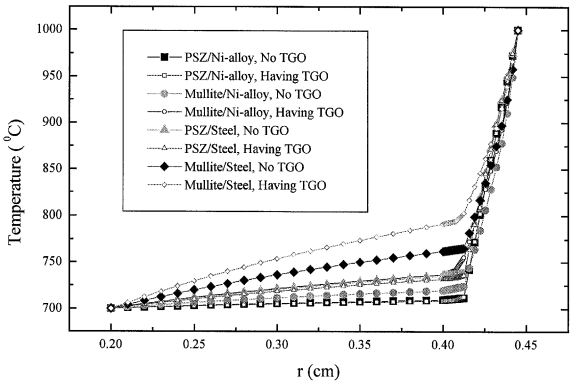

Fig. 4. Spatial distribution of temperature at time of 14 000 s.

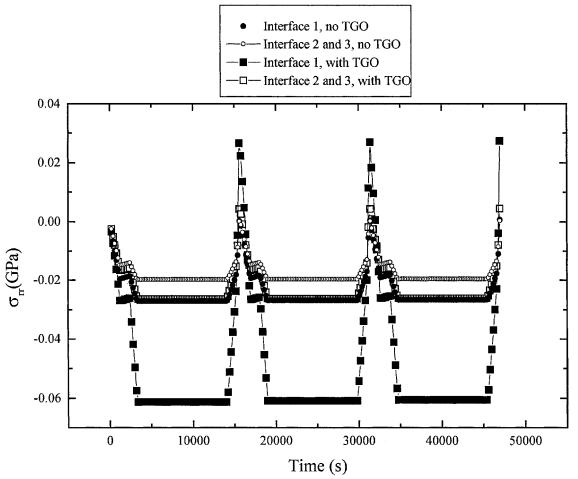

Fig. 5. Histories of radial stress σ_{rr} at interfaces 1, 2 and 3 for PSZ/Ni-alloy system at elastic state.

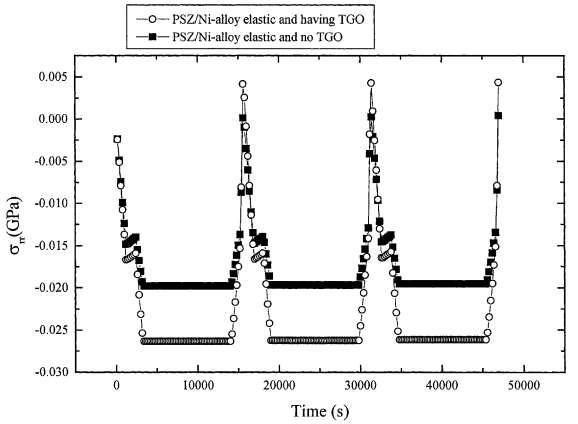

Fig. 6. Histories of radial stress σ_{rr} at interface 3 for PSZ/Ni-alloy system at elastic state with or without considering TGO.

Second, the tangent stresses are discussed. The histories of tangent stress on outer surface are shown in Fig. 8. At very early stage of heating, the tangent stresses are compressive without and with considering TGO. But the state of compressive tangent stress maintains less than 12 s. After that time, stresses are tensile on outer surface during heating and heat hold. However, the tangent stresses become compressive on the end of cooling for every heating/cooling. The compressive stresses are due to the mismatch of thermal expansion and are called residual stresses. Fig. 8 shows that the residual elastic compressive stress is very little for TGO non-considered. The residual elastic compressive stresses for TGO considered are larger than that for TGO non-considered as shown in Fig. 8. Fig. 9(a) and (b) show the spatial distribution of tangent stress for TGO non-considered and TGO considered at different time. It is seen that the maximum tensile or compressive stresses in TGO are much larger than that in substrate or bond and ceramic coating. This is due to very large Young's modulus of TGO as given in Table 3. It is very interesting to note the difference of residual tangent stress shown in Fig. 9(a) and (b). The residual stresses are tensile for TGO non-considered

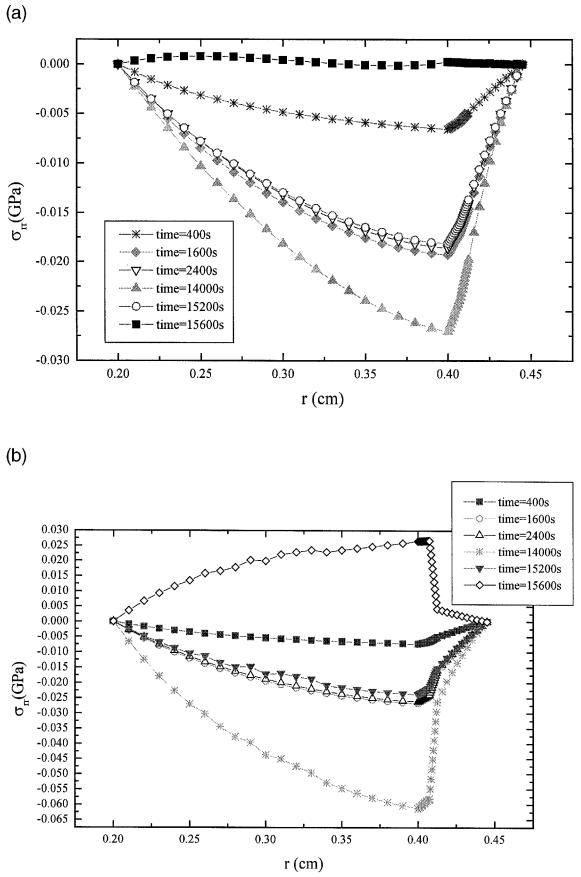

Fig. 7. Spatial distribution of radial stresses for PSZ/Ni-alloy system at elastic state at different times: (a) without considering TGO and (b) with considering TGO.

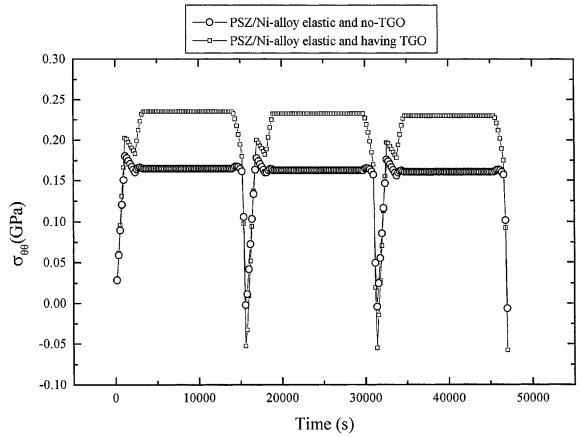

Fig. 8. Histories of tangent stress $\sigma_{\theta\theta}$ on outer surface for PSZ/Ni-alloy system at elastic state.

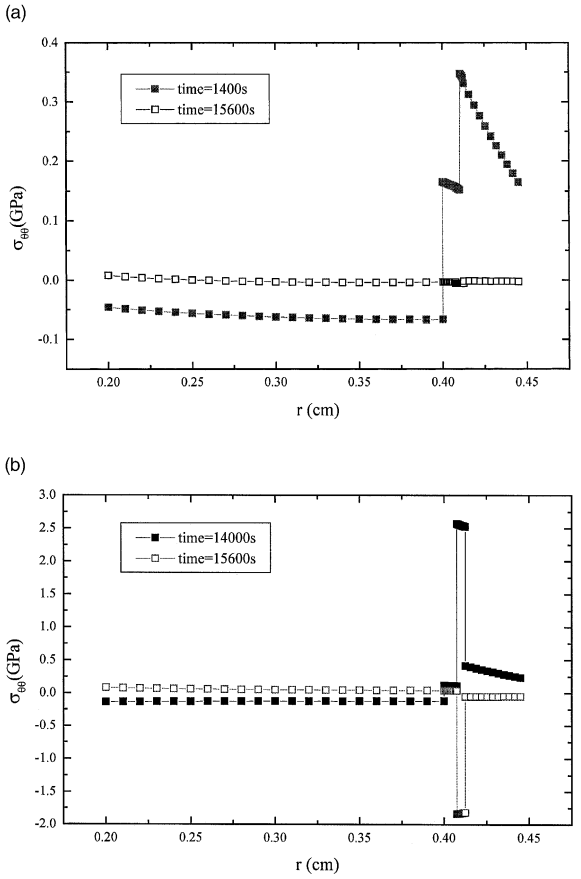

Fig. 9. Spatial distribution of tangent stress $\sigma_{\theta\theta}$ for PSZ/Ni-alloy system at elastic state at different times: (a) without considering TGO and (b) with considering TGO.

and the residual stress are compressive for TGO considered. It is concluded that TGO may largely affect the thermal stress fields. The TGO may make the residual tangent stress from tensile change to compressive.

4.6. Radial stresses for different combinations of TBC system

The spatial distributions of radial stress for different combinations of TBC system with considering TGO are shown in Fig. 10. It is noted that the radial stresses are compressive in heating and heat hold period for all combinations of TBC system. The radial stresses for all combinations of TBC systems become tensile on the end of cooling. The tensile stresses in PSZ/Ni-alloy system and Mullite/Ni-alloy system are larger than that in PSZ/Steel system and Mullite/Steel system. It is also noted that the maximum radial compressive or tensile stresses exist in TGO and bond coat. It may be concluded that the TGO and bond coat may first damage if only the radial stress is considered.

The histories of radial stresses at interfaces 1, 2 and 3 are, respectively, shown in Figs. 11 and 12 for TBC system with TGO non-considered and TGO-considered. It is noted that the compressive or tensile stresses shown in Fig. 12 are all much larger than those shown in Fig. 11. This means that the effect of TGO on

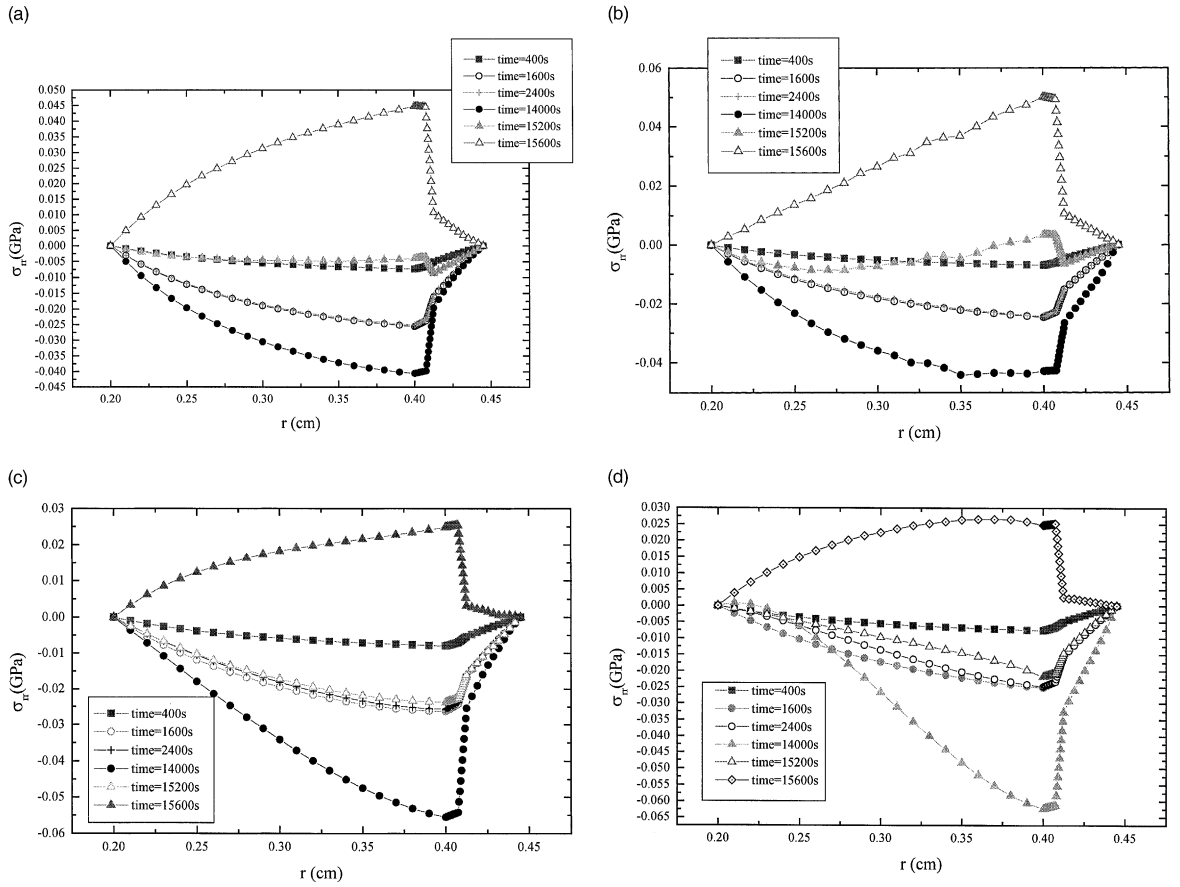

Fig. 10. Spatial distribution of radial stress with considering TGO at different times: (a) PSZ/Ni-alloy system, (b) Mullite/Ni-alloy system, (c) PSZ/Steel system, and (d) Mullite/Steel system.

thermal stresses in TBC system is very important. On the other hand, the compressive or tensile stresses for TGO effect at interface 1 are much larger than those at interface 3. Inspecting Figs. 11 and 12, it is found that there is an interesting phenomenon. We could classify the different combinations of TBC systems as two coating systems which are, named as PSZ coating system and mullite coating system. In PSZ coating system the residual radial stresses become more and more low for many cycles of heating/cooling. After some finite cycles of heating/cooling, the residual stress becomes compressive and not tensile. However, in mullite coating system, the residual radial stresses become more and more high for many cycles of heating/cooling. The residual stress is permanently tensile.

Why is there the difference of stress characterization between PSZ coating and Mullite coating? Inspecting the creep constitutive of coating, one can find that the creep rate for PSZ is much larger that for mullite. For example, at 1 h with temperature of 1000°C and equivalent stress of 1200 MPa, the creep rate for PSZ and mullite are, respectively, 3.10×10^{-7} s^{-1}, 2.48×10^{-29} s^{-1}. On the second reason, the mismatch of thermal and mechanical properties of ceramic with substrate is also very different for PSZ coating and mullite coating. For example, Dundurs' parameters $\overline{\alpha}$ and $\overline{\beta}$ defined by Dundurs (1969) can reflect the mechanical mismatch,

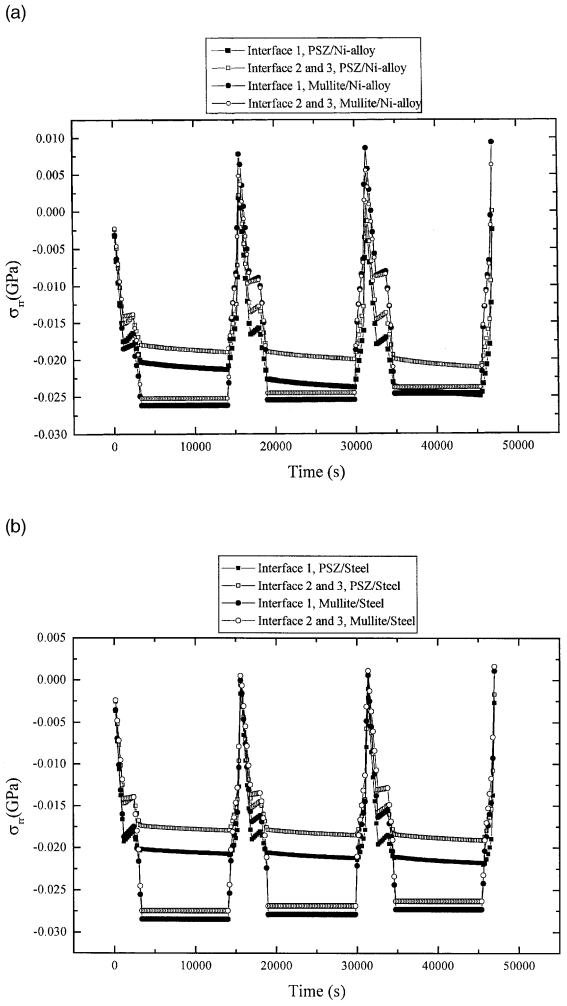

Fig. 11. Histories of radial stresses at interfaces 1, 2 and 3 with TGO non-considered: (a) Ni-alloy substrate, and (b) steel substrate.

$$\overline{\alpha} = \frac{\Gamma(\kappa_2 + 1) - (\kappa_1 + 1)}{\Gamma(\kappa_2 + 1) + (\kappa_1 + 1)}, \qquad \overline{\beta} = \frac{\Gamma(\kappa_2 - 1) - (\kappa_1 - 1)}{\Gamma(\kappa_2 + 1) + (\kappa_1 + 1)}, \tag{50}$$

where $\Gamma = \mu_1/\mu_2$, the subscripts 1 and 2 denote ceramic and substrate, respectively. By inspecting Dundurs' parameters $\overline{\alpha}$ and $\overline{\beta}$ as shown in Fig. 13(a) and (b), one finds that $\overline{\alpha}$ and $\overline{\beta}$ both decrease with the increase of interface temperature for PSZ coating system. However, $\overline{\alpha}$ and $\overline{\beta}$ both increase with the increase of interface temperature for mullite coating system. The characterizations of Dundurs' parameters $\overline{\alpha}$ and $\overline{\beta}$ depending on the interface temperature may lead to the distinct characterizations of thermal stress for PSZ coating and mullite coating systems. There should be relation of thermal stresses with Dundurs' parameters $\overline{\alpha}$ and $\overline{\beta}$. The relation is yet not known and it may be obtained by non-dimensional analysis. On the other hand, what is the thermal mismatch to reflect the distinct characterizations of thermal stress for PSZ coating and mullite coating systems? The problem will be discussed further.

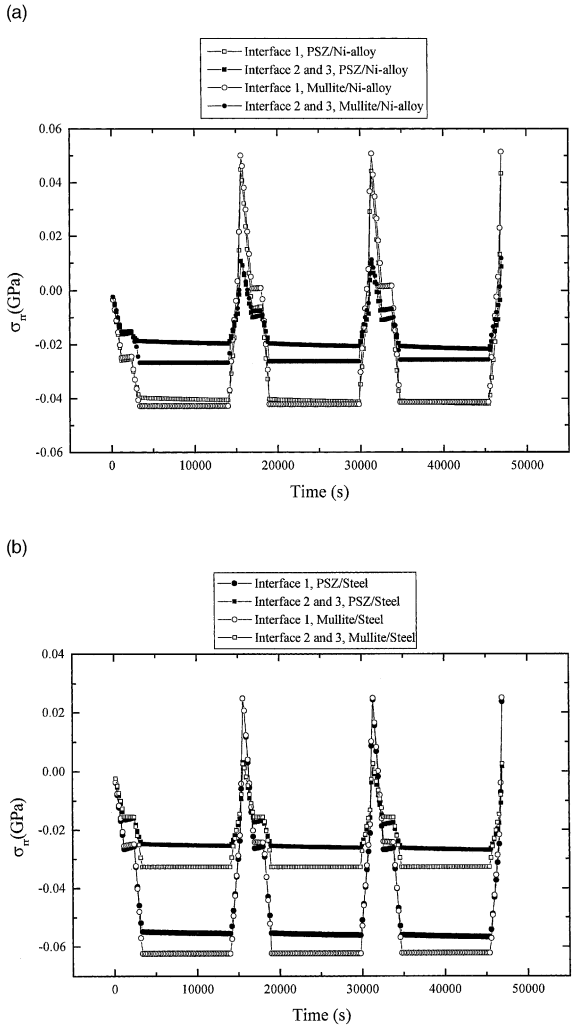

Fig. 12. Histories of radial stresses at interfaces 1, 2 and 3 with TGO considered: (a) Ni-alloy substrate, (b) Steel substrate, (c) PSZ/Steel system, and (d) Mullite/Steel system.

4.7. Tangent stresses for different combinations of TBC system

Fig. 14 shows the spatial distribution of tangent stresses for different combinations of TBC systems. It is seen that the tangent stress is not continuous across the interface. The tangent stress in one layer is different from that in other layers. First, let us inspect the tangent stress characterization in TBC system without considering TGO for the first cycle of heating/cooling. Generally, the tangent stress in ceramic coating is higher than that in bond coat or substrate in heat hold for TGO non-considered. However, the state is different for cooling period. On the end of cooling, the tangent stress in bond coat is higher than that in ceramic coating or substrate. The tangent stress in ceramic coating is tensile in the period of heat hold and that is compressive on the end of cooling. Second, let us inspect the tangent stress characterization in TBC system with considering TGO for the first cycle of heating/cooling. It is found that the tangent stress in

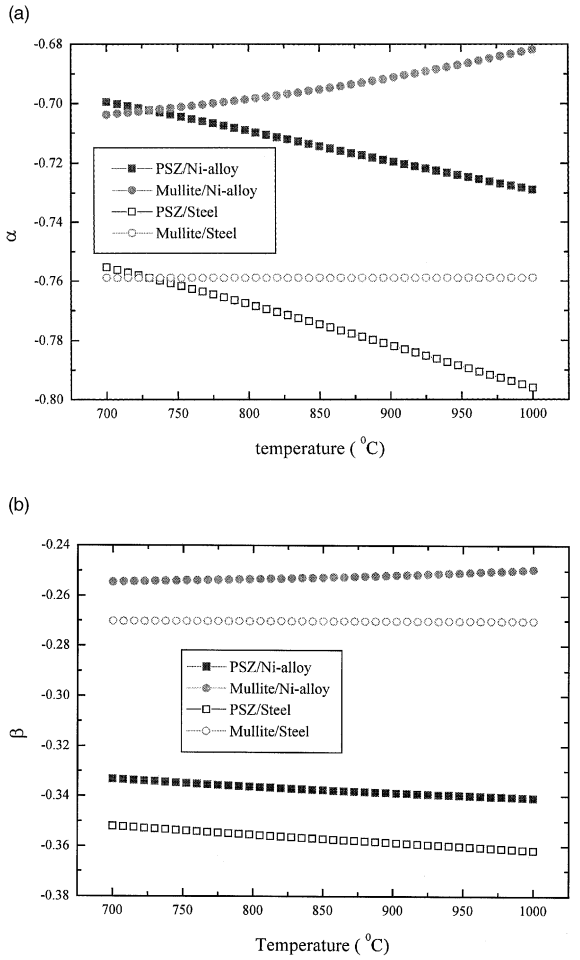

Fig. 13. The relation of Dundurs' parameters $\bar{\alpha}$ and $\bar{\beta}$ with interface temperature: Dundurs' parameters (a) $\bar{\alpha}$ and (b) $\bar{\beta}$.

TGO is much larger than that in other layers both in heat hold and on the end of cooling. The residual compressive tangent stress in ceramic coating for TGO considered is much larger than that in ceramic coating for TGO non-considered.

As discussed above for radial stress characterization, the combinations of TBC systems also can be classified as PSZ coating system and mullite coating system. Fig. 15 shows the comparison of tangent stress characterization in PSZ coating system and mullite coating system. In PSZ coating system, the residual tangent compressive stresses become more and more high for many cycles of heating/cooling. But in mullite coating system, the residual tangent is almost constant for many cycles of heating/cooling. In all TBC systems, the residual radial tensile stress is low or it is compressive. The radial stress may not cause the damage of interface. But the more and more high residual compressive tangent stress in ceramic coating may cause the ceramic coating damage in the form of delamination as studied by He et al. (1998) and Wang and Evans (1999).

The problem of delamination cracking was studied by Zhou and Hashida (1999) for the existence of radial tensile or compressive stress and temperature gradient in TBC system. The failure of TBC system is

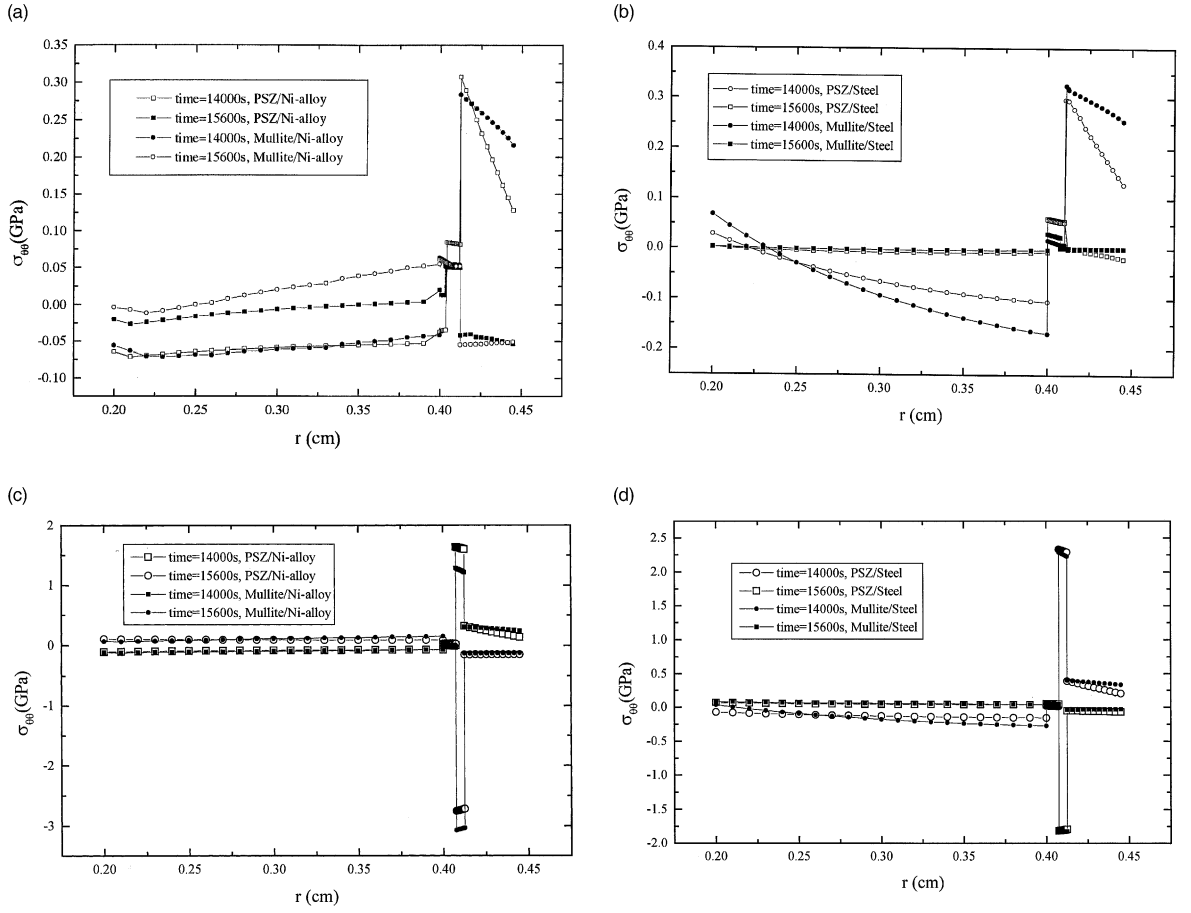

Fig. 14. Spatial distribution of tangent stresses at different times for different combinations of TBC systems: (a) and (c) Ni-alloy substrate, (b) and (d), steel substrate, where TGO is not considered in (a) and (b) and TGO is considered in (c) and (d).

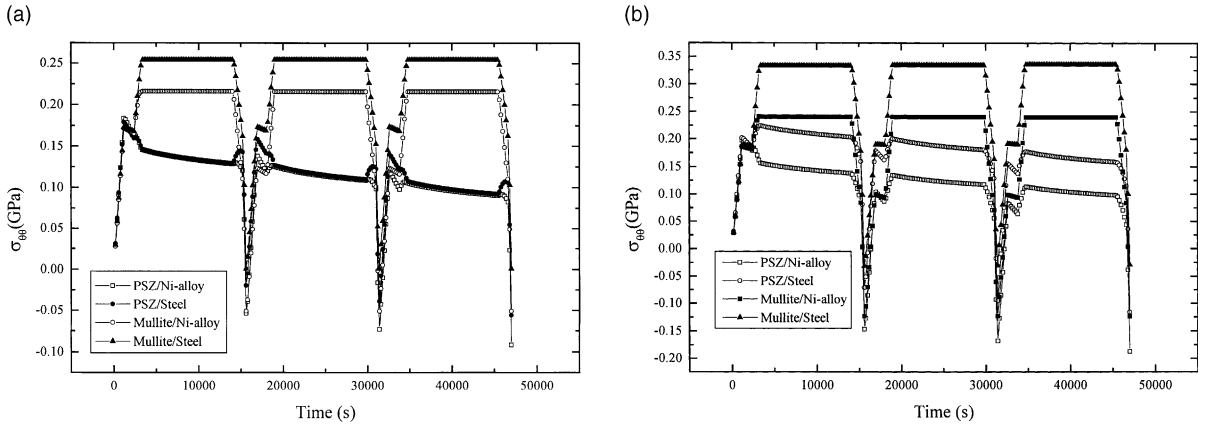

Fig. 15. Histories of tangent stresses on outer surface for different TBC systems: (a) without considering TGO and (b) with considering TGO.

the comprehensive effect of radial stress and tangent stress with temperature gradient in TBC system. Generally, it is the compressive load in ceramic coating that leads the coating delaminating for typical TBC system such as PSZ/Ni-alloy. This also means that the failure of TBC system is the non-linear coupled effect of temperature gradient, oxidation, thermal fatigue, and creep.

4.8. The effect of geometrical radius on thermal stress

Fig. 16 shows the effect of geometrical radius on thermal stress and the effect can be clearly seen. The residual radial stress is tensile for $r_0 = 0.2$ cm and that is compressive for $r_0 \geqslant 1$ cm. The residual radial compressive stress is almost constant when $r_0 \geqslant 5$ cm. The residual tangent stress is compressive for $r_0 < 5$ cm and it is tensile for $r_0 \geqslant 5$ cm. The residual tangent tensile stress is almost constant when $r_0 \geqslant 10$ cm. It is concluded that the geometrical radius not only affects the quantum of thermal stress but also affects the characterization of thermal stress. For example, the compressive tangent stress for the system in small radius may become tensile stress for the system in large radius. The change of compressive tangent stress to tensile tangent stress may largely affect the mode of crack formation and propagation, such as vertical crack or interface crack, as observed in failure experiment in TBC by laser beam thermal shock (Jian et al., 1995; Jian, 1996).

4.9. The effect of cooling rate on thermal stress

Generally, the system may encounter some special condition. In this case, the system may stop operating and the system is suddenly cooled. In order to investigate the effect of cooling rate on the TBC system failure mechanism. The radial stresses for PSZ/Ni-alloy system at different operating temperature conditions are given in this section. Fig. 17 shows the histories of radial stress at interface 3 for different outer surface temperatures and cooling time. Fig. 18 shows the residual tangent stress on outer surface after three cycles of heating/cooling.

First, it is seen that the residual radial stress is tensile for system operating at 1000°C, and it is compressive for system operating at 1200°C. The residual stress becomes more and more large after many cycles of heating/cooling for the system operating at 1200°C. However, the residual stress after 3 cycles of

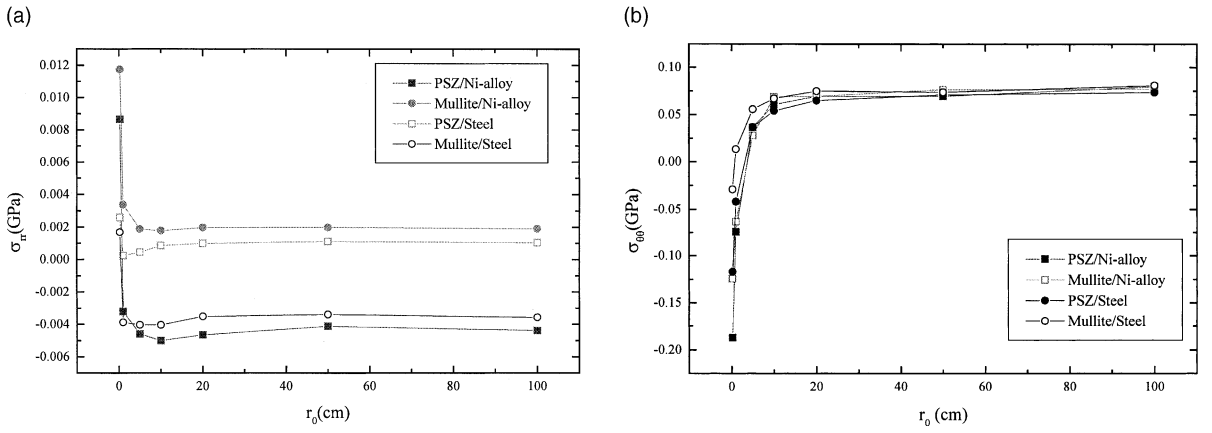

Fig. 16. The effect of geometrical radius on thermal stress, (a) residual radial stress at interface 3 on the end of cooling for three cycles of heating/cooling, (b) residual tangent stress on outer surface on the end of cooling for three cycles of heating/cooling.

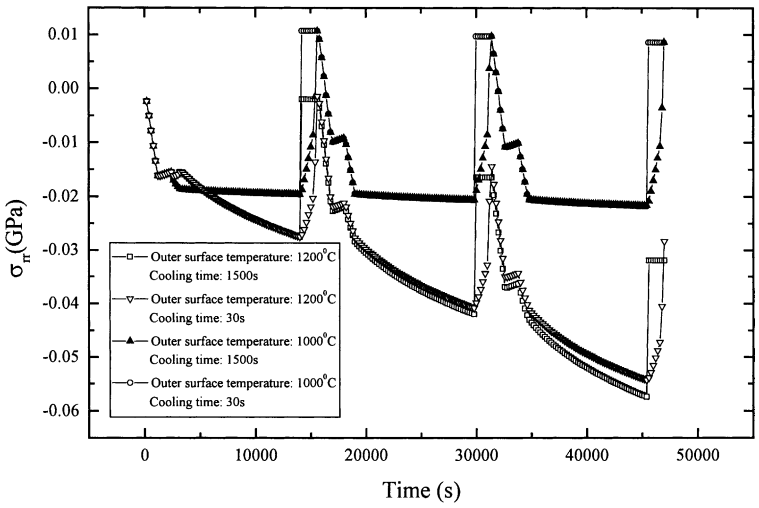

Fig. 17. Histories of radial stress at interface 3 for different outer surface temperatures and cooling time.

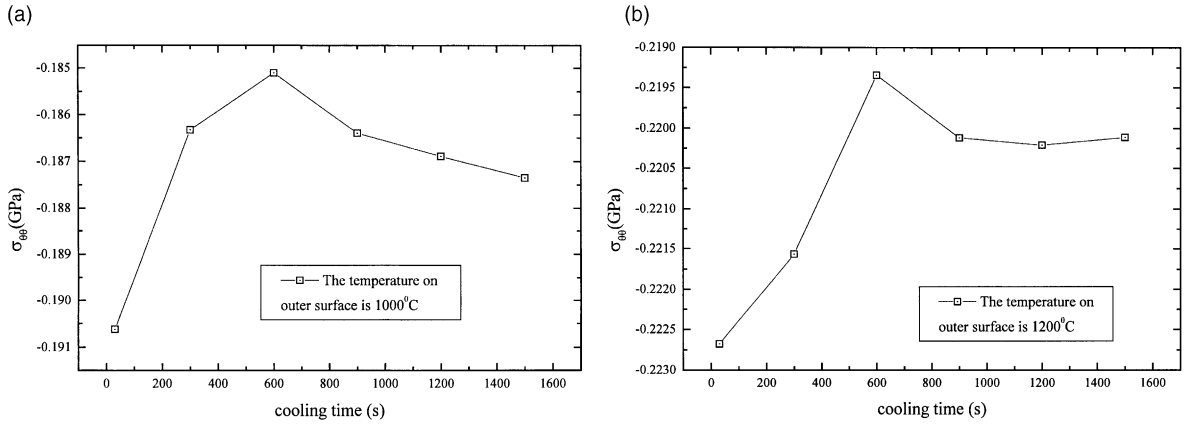

Fig. 18. Residual tangent stress on outer surface after three cycles of heating/cooling: outer surface temperature is (a) 1000°C and (b) 1200°C.

heating/cooling is almost same as that after 1 cycle of heating/cooling for the system operating at 1000°C. It is known that the creep rate is temperature dependent as shown in Eq. (39). The creep rate of ceramic coating at 1200°C is much higher than that at 1000°C. Therefore, the residual stress for system operating at high temperature is much larger than that at relative low temperature.

Second, it is seen that there is an effect of cooling rate on residual tangent stress. As shown in Fig. 18, the residual tangent stress at cooling rate of $40°C\,s^{-1}$, i.e., cooling time of 30 s is much higher than that at cooling rate of $0.8°C\,s^{-1}$, i.e., cooling time of 1500 s. The difference of residual tangent stress is not too large when cooling rate is lower than $4°C\,s^{-1}$, i.e., cooling time $t > 300$ s. There is no obvious difference for the effect of cooling rate on tangent stress when TBC system operates at 1200°C and 1000°C.

5. Concluding remarks

In the present article, the thermal stress fields in TBC system are studied. The stress fields are induced by the non-linear coupling effect of temperature gradient, oxidation, thermal fatigue, creep, and morphology of TBC system as well as cooling rate. The TBC system is assumed to be partially stabilized ZrO_2 by 8 wt.% Y_2O_3 or mullite over a NiCrAlY bond coat sprayed on nickel superalloy or steel substrate. In order to investigate the effect of different materials combinations on the failure mechanism of TBC system, four different combinations of TBC system are studied. The four systems are PSZ coating over a NiCrAlY bond coat on Ni-superalloy substrate, mullite coating over a NiCrAlY bond coat on Ni-superalloy substrate, PSZ coating over a NiCrAlY bond coat on steel substrate and mullite coating over a NiCrAlY bond coat on steel substrate. The TBC system is a composite medium with four layers in cylindrical coordinate system. First, the temperature fields for the non-homogeneous problem with energy generation in medium are analytical solved by using Taylor transformation and Green's function approach. Second, the analytical solutions for thermal stress fields in composite medium are obtained when eigenstrain rate is taken into consideration. Third, the constitutive equations, such as the creep of ceramic coating (PSZ and mullite) and substrate (Ni-superalloy), plasticity of bond coat are given by a general formula. Fourth, the thermal grown oxidation and the temperature dependence of thermal–mechanical parameters are taken into consideration.

The calculated results of temperature fields and thermal stresses fields are given and the related results are discussed. When TGO is not considered, the highest temperature difference for substrate exists in mullite/steel system and the least temperature difference exists in PSZ/Ni-alloy system. The highest temperature encountered to substrate is 709.57°C for PSZ/Ni-alloy system, however, it is 761.97°C for mullite/steel system. Therefore, the PSZ/Ni-alloy system is an optimum combination only if temperature field is considered for TBC system operating at above typical condition. TGO does not affect the temperature fields in PSZ coating systems. But it has effect on temperature fields in mullite coating systems. It makes the temperature difference be high in substrate.

The elastic stress fields for PSZ/Ni-alloy show that the radial stress is compressive and tangent stress is tensile in the period of heating and heat hold. The maximum values for compressive or tensile radial stresses exist at interfaces. The residual stresses are very little when TGO is not considered. The residual stress with TGO considered is larger than that with TGO non-considered. It is very interesting to conclude that the TGO may make the residual tangent stress from tensile to compressive.

The characterization of thermal stresses in PSZ coating system is very different from that in mullite coating system. The residual radial stresses become more and more low for many cycles of heating/cooling in PSZ/Ni-alloy system. After some finite cycles of heating/cooling, the residual stress becomes compressive and not tensile. However, the residual radial stresses become more and more high for many cycles of heating/cooling in mullite coating system. The residual stress is permanently tensile. In PSZ coating system, the residual tangent compressive stresses become more and more high for many cycles of heating/cooling. But in mullite coating class, the residual tangent is almost constant for many cycles of heating/cooling. The difference of stress characterization in PSZ coating system and mullite coating system is discussed. It may be due to the difference of mechanical behavior, such as creep, thermal mismatch and thermal expansion coefficients as well as mechanical mismatch, which is reflected by Dundurs' parameters $\overline{\alpha}$ and $\overline{\beta}$.

The effect of geometrical radius of TBC system on thermal stress is very obvious. The geometrical radius not only affects the quantum of thermal stress but also affects the characterization of thermal stress. The compressive tangent stress for the system in small radius may become tensile stress for the system in large radius. The change of compressive tangent stress to tensile tangent stress may largely affect the mode of crack formation and propagation, such as vertical crack or interface crack, as observed in failure experiment in TBC system by laser beam thermal shock (Jian et al., 1995; Jian, 1996). The effect of cooling rate on residual stress is studied. The effect is due to the high creep rate of ceramic coating operating at high temperature and the effect is not large for system operating at relatively low temperature.

In conclusion, the failure of TBC system is the comprehensive effect of radial stress and tangent stress with temperature gradient in TBC system. Generally, it is the compressive load in ceramic coating that leads to the coating delaminating. This also means that the failure of TBC system is the non-linear coupled effect of temperature gradient, oxidation, thermal fatigue, creep, morphology of TBC system as well as cooling rate.

Acknowledgements

The collaborative research for foreign researchers in Japan was provided to first author Y.C.Z by JSPS (Japan Society for the Promotion of Science). This support is gratefully acknowledged. A part of this work was supported by the Grant-in-Aid for COE (Center of Excellence) Research (no. 11CE2003), The Ministry of Education, Science, Sports and Culture. The authors express their appreciation to the grant.

Appendix A

In this appendix, the functions $\phi_i(r)$, $\psi_i(r)$ and $\vartheta_i(r,t)$ in Eq. (14) are given in the following. First the function $\phi_i(r)$ is given as

$$\phi_i(r) = A_i + B_i \ln\left(\frac{r}{r_1}\right), \quad i = 1,2,\ldots,M, \tag{A.1}$$

where the $2M$ coefficients A_i and B_i for $i = 1,2,\ldots,M$ are determined by the following $2M$ linear equations:

$$A_1 - B_1 \frac{1}{r_1}\frac{k_1}{h_1} = 1, \tag{A.2}$$

$$A_i - A_{i+1} + B_i\left[\ln\frac{r_{i+1}}{r_1} + \frac{k_i(T_0)}{h_{i+1}}\frac{1}{r_{i+1}}\right] - B_{i+1}\ln\frac{r_{i+1}}{r_1} = 0, \quad i = 1,2,\ldots,M-1, \tag{A.3}$$

$$B_i - B_{i+1}\frac{k_i(T_0)}{k_{i+1}(T_0)} = 0, \quad i = 1,2,\ldots,M-1, \tag{A.4}$$

$$A_M + B_M\left(\frac{k_M}{h_{M+1}}\frac{1}{r_{M+1}} + \ln\frac{r_{M+1}}{r_1}\right) = 0. \tag{A.5}$$

Second, the function $\psi_i(r)$ is given as

$$\psi_i(r) = C_i + D_i \ln\frac{r}{r_1}, \quad i = 1,2,\ldots,M, \tag{A.6}$$

where the $2M$ coefficients C_i and D_i for $i = 1,2,\ldots,M$ are determined by the following $2M$ linear equations:

$$C_1 - D_1 \frac{1}{r_1}\frac{k_1}{h_1} = 0, \tag{A.7}$$

$$C_i - C_{i+1} + D_i\left[\ln\frac{r_{i+1}}{r_1} + \frac{k_i(T_0)}{h_{i+1}}\frac{1}{r_{i+1}}\right] - D_{i+1}\ln\frac{r_{i+1}}{r_1} = 0, \quad i = 1,2,\ldots,M-1, \tag{A.8}$$

$$D_i - D_{i+1}\frac{k_i(T_0)}{k_{i+1}(T_0)} = 0, \quad i = 1,2,\ldots,M-1, \tag{A.9}$$

$$C_M + D_M\left(\frac{k_M}{h_{M+1}}\frac{1}{r_{M+1}} + \ln\frac{r_{M+1}}{r_1}\right) = 1. \tag{A.10}$$

Third, the function $\vartheta_i(r,t)$ is given as

$$\vartheta_i(r,t) = \sum_{j=1}^{M}\left\{\int_{r_j}^{r_{j+1}} \zeta\left|G_{ij}(r,t|\zeta,\tau)\right|_{\tau=0}\gamma_j^*(\zeta)\,\mathrm{d}\zeta + \int_0^t \mathrm{d}\tau\int_{x_j}^{x_{j+1}} \zeta G_{ij}(x,t|\zeta,\tau)\left[\frac{b_j(T_j)}{k_j(T_0)}g_j^*(\zeta,\tau)\right]\mathrm{d}\zeta\right\}, \tag{A.11}$$
$$r_i < r < r_{i+1},\quad i = 1,2,\ldots,M,$$

where

$$g_i^*(r,t) = g_i(r,t) - \frac{k_i(T_0)}{b_i(T_i)}[\phi_i(r)f_1'(t) + \psi_i(r)f_M', (t)], \tag{A.12}$$

$$\gamma_i^*(r) = \gamma_i(r) - [\phi_i(r)f_1(0) + \psi_i(r)f_{M+1}(0)]. \tag{A.13}$$

In expression (A.12), the primes denote differentiation with respect to t. The composite medium Green's function $G_{ij}(r,t|\zeta,\tau)$ is defined as

$$G_{ij}(r,t|\zeta,\tau) = \sum_{n=1}^{\infty}\mathrm{e}^{-\beta_n^2(t-\tau)}\frac{1}{N_n}\frac{k_j(T_0)}{b_j(T_j)}\Phi_{in}(r)\Phi_{jn}(\zeta). \tag{A.14}$$

The norm N_n is given by

$$N_n = \sum_{j=1}^{M}\frac{k_j(T_0)}{b_j(T_j)}\int_{x_j}^{x_{j+1}}\zeta\Phi_{jn}^2(\zeta)\,\mathrm{d}\zeta. \tag{A.15}$$

In the above presentations, $\Phi_{in}(r)$ and $\Phi_{jn}(r)$ are the eigenfunctions which are given by

$$\Phi_{in}(r) = U_{in}J_0\left(\frac{\beta_n}{\sqrt{b_i(T_i)}}r\right) + V_{in}Y_0\left(\frac{\beta_n}{\sqrt{b_i(T_i)}}r\right), \tag{A.16}$$

where $J_0(x)$ and $Y_0(x)$ are zero-order Bessel function of the first and second kind, respectively. The $2M$ coefficients U_{in} and V_{in} for $i = 1,2,\ldots,M$ are determined by the following $2M$ linear equations:

$$U_{1n}[-k_1J_0'(x_{1n}r_1) + h_1J_0(x_{1n}r_1)] + V_{1n}[-k_1Y_0'(x_{1n}r_1) + h_1Y_0(x_{1n}r_1)] = 0, \tag{A.17}$$

$$\begin{aligned}&U_{in}[-k_iJ_0'(x_{in}r_{i+1}) - h_{i+1}J_0(x_{in}r_{i+1})] + V_{in}[-k_iY_0'(x_{in}r_{i+1}) - h_{i+1}Y_0(x_{in}r_{i+1})]\\ &\quad + U_{i+1,n}[h_{i+1}J_0(x_{i+1,n}r_{i+1})] + V_{i+1,n}[h_{i+1}Y_0(x_{i+1,n}r_{i+1})] = 0,\end{aligned} \tag{A.18}$$

$$U_{in}[k_iJ_0'(x_{in}r_{i+1})] + V_{in}[k_iY_0'(x_{in}r_{i+1})] - U_{i+1,n}[k_{i+1}J_0'(x_{i+1,n}r_{i+1})] - V_{i+1,n}[k_{i+1}Y_0'(x_{i+1,n}r_{i+1})] = 0, \tag{A.19}$$

$$U_{Mn}[k_MJ_0'(x_{Mn}r_{M+1}) + h_{M+1}J_0(x_{Mn}r_{M+1})] + V_{Mn}[k_MY_0'(x_{Mn}r_{M+1}) + h_{M+1}Y_0(x_{Mn}r_{M+1})] = 0. \tag{A.20}$$

In the above $2M$ linear equations, $A_{1n} = 1$ and $x_{in} = (\beta_n/\sqrt{b_i(T_i)})$. The primes denote differentiation with respect to r. The transcendental equation for the determination of the eigenvalues $\beta_1 < \beta_2 < \cdots < \beta_n < \cdots$ is obtained from the requirement that the determinant of the coefficients in the system of Eqs. (A.16)–(A.20) vanish.

Appendix B

In this appendix, $2M$ constants A_i and B_i for $i = 1, 2, \ldots, M$ in Eqs. (21) and (23) are determined by the following $2M$ linear equations:

$$A_1 + \frac{1}{2}(1-\kappa_1)\frac{B_1}{r_1^2} = -C_1(r_1,t) - \frac{1}{2}(1-\kappa_1)\frac{D_1(r_1,t)}{r_1^2} + E_1(r_1,t), \tag{B.1}$$

$$\begin{aligned} &A_i + \frac{1}{2}(1-\kappa_i)\frac{B_i}{r_{i+1}^2} - \frac{\mu_{i+1}}{\mu_i}\,\frac{\kappa_i - 1}{\kappa_{i+1} - 1}\left[A_{i+1} + \frac{1}{2}(1-\kappa_{i+1})\frac{B_{i+1}}{r_{i+1}^2}\right] \\ &\quad = -\left[C_i(r_{i+1},t) + \frac{1}{2}(1-\kappa_i)\frac{D_i(r_{i+1},t)}{r_{i+1}^2} - E_i(r_{i+1},t)\right] + \frac{\mu_{i+1}}{\mu_i}\,\frac{\kappa_i - 1}{\kappa_{i+1} - 1}\left[C_{i+1}(r_{i+1},t)\right. \\ &\qquad \left. + \frac{1}{2}(1-\kappa_{i+1})\frac{D_{i+1}(r_{i+1},t)}{r_{i+1}^2} - E_{i+1}(r_{i+1},t)\right], \quad i = 1, 2, \ldots, M-1, \end{aligned} \tag{B.2}$$

$$A_i + \frac{B_i}{r_{i+1}^2} - A_{i+1} - \frac{B_{i+1}}{r_{i+1}^2} = -C_i(r_{i+1},t) - \frac{D_i(r_{i+1},t)}{r_{i+1}^2} + C_{i+1}(r_{i+1},t) + \frac{D_{i+1}(r_{i+1},t)}{r_{i+1}^2}, \quad i = 1, 2, \ldots, M-1, \tag{B.3}$$

$$A_M + \frac{1}{2}(1-\kappa_M)\frac{B_M}{r_{M+1}^2} = -C_M(r_{M+1},t) - \frac{1}{2}(1-\kappa_{M+1})\frac{D_M(r_{M+1},t)}{r_{M+1}^2} + E_M(r_{M+1},t). \tag{B.4}$$

References

Amagasa, S., Shimomura, K., et al., 1994. Study on the turbine vane and blade for a 1500°C class industrial gas turbine. Trans. ASME J. Engng. Gas Turbines Power 116 (3), 597–604.

An, K., Ravichandran, K.S., et al., 1999. Microstructure, texture, and thermal conductivity of single-layer and multilayer thermal barrier coatings of Y_2O_3-stabilized ZrO_2 and Al_2O_3 made by physical vapor deposition. J. Am. Ceram. Soc. 82 (2), 399–406.

Bartlett, A.H., Maschio, R.D., 1995. Failure Mechanisms of a zirconia-8wt.% yttria thermal barrier coating. J. Am. Ceram. Soc. 78 (4), 1018–1024.

Bernstein, H.L., Allen, J.M., 1992. Analysis of cracked gas turbine blades. J. Engng. Gas Turbines Power 114 (2), 293–301.

Betteridge, W., 1984. Nickel and its Alloys. Ellis Horwood, Chichester, UK.

Chaudhury, Z.A., Newaz, G.M., Nusier, S.Q., Ahmed, T., 1997. Interfacial damage in EB-PVD thermal barrier coatings due to thermal cycling. Mater. Sci. Engng. 231A, 34–41.

Cheng, J., Jordan, E.H., Barber, B., Gell, M., 1998. Thermal/residual stress in an electron beam physical vapor deposited thermal barrier coating system. Acta Mater. 46 (16), 5839–5850.

Chung, B.T.F., Kermani, M.M., et al., 1985. Heat transfer in thermal barrier coated rods with circumferential and radial temperature gradients. Trans. ASME J. Engng. Gas Turbines Power 107 (1), 135–141.

Cruse, T.A., Stewart, S.E., Ortiz, M., 1988. Thermal barrier coating life prediction model development. J. Engng. Gas Turbines Power 110 (4), 610–616.

DeMasi-Marcin, J.T., Sheffler, K.D., Bose, S., 1990. Mechanisms of degradation and failure in a plasma-deposited thermal barrier coating. J. Engng. Gas Turbines Power 112 (4), 521–526.

Dundurs, J., 1969. Discussion of a paper by D.B. Bogy. Trans. ASME J. Appl. Mech. 36 (3), 650–652.

Dundurs, J., 1990. Boundary conditions at interfaces. In: Weng, G.J., et al. (Eds.), Micromechanics and Inhomogeneous. Springer, Berlin, pp. 109–114.

Gell, M., et al., 1999. Mechanism of spallation in platinum aluminide/electron beam physical vapor-deposited thermal barrier coatings. Metall. Trans. A 30 (2), 427–435.

Glandus, J.C., Tranchand, V., 1993. Thermal shock by water quench: numerical simulation. In: Schneider, G.A., Petzow, G. (Eds.), Thermal Shock and Thermal Fatigue Behavior of Advanced Ceramics. Kluwer Academic Publishers, Dordrecht, pp. 307–316.

Hasselman, D.P.H., Johnson, L.F., Bentsen, L.D., Syed, R., Lee, H.L., Swain, M.V., 1987. Thermal diffusivity and conductivity of dense polycrystalline ZrO_2 ceramic: a survey. Am. Ceram. Soc. Bull. 66 (5), 799–806.

He, M.Y., Evans, A.G., Hutchinson, J.W., 1998. Effects of morphology on the decohesion of compressed thin films. Mater. Sci. Engng. A 245, 168–181.

Hyde, T.H., Xia, L., Becker, A.A., Sun, W., 1997. Fatigue, creep and creep/fatigue behaviour of a nickel base superalloy at 700°C. Fatigue Fract. Engng. Mater. Struct. 20 (9), 1295–1303.

Itoh, Y., Takahashi, M., Ishiwata, Y., Nagata, K., 1988. Basic study of oxidation behavior of zirconia thermal barrier coating at high-temperature. J. Soc. Mater. Sci. Japan 47 (7), 665–671 (in Japanese).

Jian, C.Y., 1996. Study on Evaluation Method of Ceramic Coating System for Gas Turbine Rotator Blades. Doctoral Thesis, Tohoku University, Japan.

Jian, C.Y., Hashida, T., et al., 1995. Thermal shock and fatigue resistance evaluation of functionally graded coating for gas turbine blades by laser heating method. Compos. Engng. 5 (7), 879–889.

Kokini, K., Takeuchi, Y.R., Choules, B.D., 1996. Surface thermal cracking of thermal barrier coatings owing to stress relaxation: zirconia vs. mullite. Surface Coat. Technol. 82, 77–82.

Meier, S.M., Nissley, D.M., Sheffler, K.D., Cruse, T.A., 1992. Thermal barrier coating life prediction model development. J. Engng. Gas Turbines Power 114 (2), 258–263.

Miller, R.A., 1989. Life modeling of thermal barrier coatings for aircraft gas turbine engines. J. Engng. Gas Turbines Power 111 (2), 301–305.

Mura, T., 1982. Micromechanics of defects in Solid. Martinus Nijhoff Publishers, The Hague.

Newaz, G.M., Nusier, S.Q., Chaudhury, Z.A., 1998. Damage accumulation mechanisms in thermal barrier coatings. J. Engng. Mater. Tech. 120 (2), 149–153.

Nusier, S.Q., Newaz, G.M., 1988. Transient residual stresses in thermal barrier coatings: analytical and numerical results. Trans. ASME J. Appl. Mech. 65 (2), 346–353.

Ogawa, K., Minkov, D., Shoji, T., Sato, M., Hashimoto, H., 1999. NDE of degradation of thermal barrier coating by means of impedance spectroscopy. NDTE Int. 32 (3), 177–185.

Özisik, M.N., 1993. Heat Conduction, second ed. Wiley, New York.

Rejda, E.F., Socie, D.F., Beardsley, B., 1997. Fatigue behavior of a plasma-sprayed 8% Y_2O_3–ZrO_2 thermal barrier coating. Fatigue Fract. Engng. Mater. Struct. 20 (7), 1043–1050.

Rohde, M., 1997. Measuring and modeling thermal conductivity in thin films and microstructures. High Temp. High Pressures 29 (2), 171–176.

Schneider, H., Okada, K., Pask, J.A., 1994. Mullite and Mullite Ceramics. Wiley, New York.

Tabuchi, M., Kubo, K., Yagi, K., Yokobori Jr., A.T., Fuji, A., 1999. Results of a Japanese round robin on creep crack growth evaluation methods for Ni-base superalloys. Engng. Fract. Mech. 62 (1), 47–60.

Takeuchi, Y.R., Kokini, K., 1994. Thermal fracture of multilayer ceramic thermal barrier coatings. Trans. ASME J. Engng. Gas Turbines Power 116 (1), 266–271.

Tawancy, H.M., Sridhar, N., et al., 1998. Failure mechanism of a thermal barrier coating system on a nickel-base superalloy. J. Mater. Sci. 33 (3), 681–686.

Taylor, R.E., 1998. Thermal conductivity determinations of thermal barrier coatings. Mater. Sci. Engng. 245A, 160–167.

Thurn, G., Schneider, G.A., Aldinger, F., 1997. High-temperature deformation of plasma-sprayed ZrO_2 thermal barrier coatings. Mater. Sci. Eng. 233A, 176–182.

Tolpygo, V.K., Dryden, J.R., Clarke, D.R., 1998. Determination of the growth stress and strain in α-Al_2O_3 scales during the oxidation of Fe–22Cr–4.8Al–0.3Y alloy. Acta Mater. 46 (3), 927–937.

Wang, J.S., Evans, A.G., 1999. Effects of strain cycling on buckling, cracking and spalling of a thermally grown alumina on a nickel-based bond coat. Acta Mater. 47 (2), 699–710.

Wesling, K.F., Socie, D.F., Beardsley, B., 1994. Fatigue of thick thermal barrier coatings. J. Am. Ceram. Soc. 77 (7), 1863.

Wu, B.C., Chang, E., et al., 1989. Degradation mechanisms of ZrO_2-8 wt.% Y_2O_3/Ni–22Cr–10Al–1Y thermal barrier coatings. J. Am. Ceram. Soc. 72 (2), 212–218.

Wu, B.C., Chang, E., et al., 1990. The oxide pegging spalling mechanism and spalling modes of ZrO_2 8 wt.% Y_2O_3/Ni–22Cr–10Al–1Y thermal barrier coatings under various operating conditions. J. Mater. Sci. 25 (2A), 1112–1119.

Yuri, I., Hisamatsu, T., Watanabe, K., Etori, Y., 1997. Structural design and high pressure test of a ceramic combustor for 1500°C class industrial gas turbine. Trans. ASME J. Engng Gas Turbines Power 119 (3), 506–511.

Zhou, Y.C., Hashida, T., 1999. Delamination cracking in thermal barrier coating syste, submitted for publication.

Zhou, Y.C., Duan, Z.P., Yan, X.H., 1997. Thermal stress wave and spallation induced by an electron beam. Int. J. Impact Engng. 19 (7), 603–614.

Zhu, D.M., Miller, R.A., 1998. Investigation of thermal high cycle and low cycle fatigue mechanisms of thick thermal barrier coatings. Mater. Sci. Engng. 245A, 212–223.

Zhu, D.M., Miller, R.A., 1999. Determination of creep behavior of thermal barrier coatings under laser imposed high thermal and stress gradient conditions. J. Mater. Res. 14 (1), 146–161.